RYERSON UNIVERSITY

FACULTY OF ENGINEERING, ARCHITECTURE AND SCIENCE

DEPARTMENT OF AEROSPACE ENGINEERING

Development of a Polymer Extrusion System to Manufacture Recycled Bioplastic Composites for Additive Manufacturing

Jordan J. W. Kalman

AER870 Aerospace Engineering Thesis – Final Report

Faculty Advisor: Dr. Kazem Fayazbakhsh

Date: April 13, 2020

Acknowledgements

The author would like to acknowledge the support of McGill Structures and Composite Materials Laboratory including PhD candidate Mr. Rahimizadeh for providing the composite pellets and the testing of the manufactured coupons. Special thanks to Mr. Samuel Woolsey for developing the software package for the feedback control system. Lastly, the author would like to extend thanks to Dr. Kazem Fayazbakhsh, FRAMES, and the aerospace engineering department for the support of this undergraduate thesis project.

Abstract

The research validates the use of recycled end-of-life wind turbine blade fiberglass to improve the mechanical strength of a thermoplastic in collaboration with McGill University. The critical fiber length glass fibers from wind turbine blades are reclaimed through a mechanical grinding process, incorporated with polylactic acid (PLA) in a twin-screw extruder to produce composite pellets and manufactured into filament via a single-screw extrusion system. This filament is used as feedstock for standard fused filament fabrication (FFF) 3D printers to manufacture ASTM standard tensile specimens: D638-14. Reinforced thermoplastic filaments with varying fiber content ranging from 3%-10% are manufactured using this process. It was found that the long fiber reinforced PLA provided a 20% increase in tensile strength and a 28% increase in the stiffness compared to the pure PLA specimens. The increased strength and stiffness can allow the material to be used in smaller quantities when replacing a given thermoplastic material. This material could be beneficial for both rapid prototyping and application-specific products. In addition to the issues faced with the waste management of wind turbines, so too is the textile waste caused by the improper disposal of clothing. To address the issues faced with improper disposal of clothing, a material characterization method for analyzing the draping behaviour of flexible 3D printed textiles was initiated. Pairing an extrusion system with 3D printing allows for the most rapid development of both a specialized material and engineering solution. Looking to the future of the textile industry, it is crucial that sustainable recycling and manufacturing processes are used to create a better future for the generations to come.

Keywords: Sustainability, Recycling, The Wind Energy Industry, Wind Turbine Blades, Lifecycle Analysis, Circular Economy, 3D Printing, Additive Manufacturing, Bioplastic, Polylactic Acid, Extrusion, Single-Screw Extruder, Fiber Reinforced Filaments, ASTM D638 Coupons.

Table of Contents

Table of Figures

List of Tables

1.0 Introduction

The purpose of this report is to present the findings of the development of a single-screw polymer extrusion system and the results found from testing recycled-fiberglass reinforced thermoplastic ASTM D638-14 coupons with varying fiber percentage. The fiberglass was reclaimed from end-of-life wind turbine blades which are otherwise landfilled or incinerated. This is a pressing issue that is a global concern for the present and the future. By 2050, the global annual turbine blade waste is expected to reach 2.9 Mt each year [1]. If this material can be utilized to improve the mechanical performance of a new material, it can be used rather than wasted. The focus of the study was on the effects of critical fiber length to improve the mechanical strength. Varying the fiber percentage by weight was investigated as follows: 3%, 5% and 10%. Furthermore, a secondary study was initiated on another potential application: addressing the current textile waste issues in the fashion industry. A preliminary draping analysis study was performed to develop a systematic method to characterize the draping characteristics of flexible 3D printed textiles.

Recycling of Wind Turbine Blades

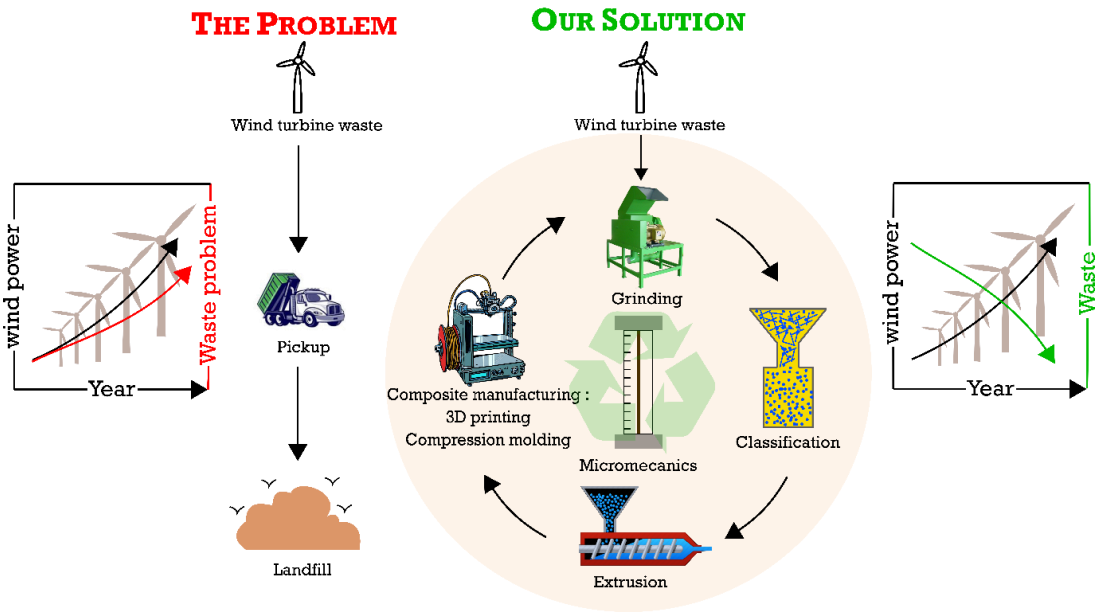

Figure 1. Novel recycling solution for processing end-of-service wind turbine blades.

The figure was produced by the corresponding author of a series of papers published in collaboration with McGill, Mr. Rahimizadeh. The figure outlines the identified problem and the proposed solution to recycle otherwise landfilled wind turbine blades. This process can be scaled up to an industrial scale to recycle the current and future demand created by the growing wind turbine waste.

1.1 Theory

1.1.1 Bioplastic

A bioplastic is typically a thermoplastic polymer synthesized from biological substances rather than a petroleum-based process [2]. A thermoplastic is a type of polymer that can be melted into a form and re-melted without chemical degradation. In contrast, a thermoset polymer such as an epoxy resin cannot be re-melted and reformed due to cross-linking in the molecular structure of the polymer chains. Bioplastics provide an alternative polymer material and decrease the dependency on fossil fuel for polymer synthesis. By using renewable polymer feedstock, a decrease in the demand for fossil fuel is required to maintain the production rate. A clear advantage of using a bioplastic is the reduced impact on pollution. When fossil fuel derived products reach the end of their lifecycle, CO_2 is released back into the atmosphere. The largest contributor to climate change has long been known to be fossil fuels. However, the dependency on their use is far-reaching and must therefore be phased out in systematic stages. Polymer production, use, and recycling is a very crucial process where fossil fuel-based polymers can be replaced with bioplastics. However, for a bioplastic to be classified as sustainable, renewable energy sources must be used for their processing, production and distribution. Bio-thermoplastics paired with renewable energy sources provide a promising solution to achieving a true circular economy. In order to achieve this, a systematic approach must be used to collect, process, manufacture and recycle these feedstocks. Guidelines have been proposed by several investigations on the mass use of bioplastics in everyday products. The primary goal outlined by these studies focuses on encouraging the development and use of bioplastics that are both environmentally safe and sustainably sourced [3]. Early initiatives include reducing the amount of material used in everyday packaging and the elimination of single-use products without recyclability or biodegradability. Fossil fuel-based feedstocks have the potential to be completely replaced with bioplastic counterparts with desired mechanical properties. ASTM standard test methods provide the necessary testing means to rigorously characterize these materials.

1.1.2 Polylactic Acid (PLA)

Polylactic acid (PLA) is a biodegradable thermoplastic produced from renewable agricultural sources such as corn and sugarcane [4]. However, its biodegradability is slow and requires either industrial composting processes or anaerobic digestion to facilitate rapid decomposition. PLA has mechanical characteristics comparable to the following thermoplastics: polystyrene (PS), polypropylene (PP), and polyethylene (PE). Although these polymers are also thermoplastics, they are all synthesized from fossil fuel-based sources. PLA is among the most widely available and used feedstock material for FFF 3D printing.

1.1.3 Ingeo Biopolymer 4043D

PLA was identified to satisfy the preliminary requirements of being both a suitably sustainable bioplastic in addition to being compatible with 3D printing. Additionally, PLA has been a major focus in literature with numerous publications studying its mechanical performance and general characteristics. To manufacture the recycled composite materials, a pure PLA feedstock was selected to be Ingeo 4043D by *NatureWorks* [5]. This feedstock material is a brand name of high-grade PLA pellets which is often used by 3D printing filament manufacturers. Below, the physical appearance is shown in addition to a table containing chemical properties.

Figure 2. Ingeo 4043D (PLA) pellets.

Table 1. Material properties summary for Ingeo 4034D. [5]

Processing Temperature Profile [4]		
Melt Temp.	410°F	210°C
Feed Throat	113°F	45°C
Feed Temp.	355°F	180°C
Compression Section	375°F	190°C
Metering Section	390°F	200°C
Adapter	390°F	200°C
Die	390°F	200°C
Screw Speed	20-100 rpm	
Filament Diameter Inspection (on-line)	Essential for quality monofilament (+/- 3% max. deviation)	
3D Printing Temp.		190-230°C
Print Bed Temp.		None needed. (or 50-70°C if applicable)

Typical Material Properties [1]		
Physical Properties	**Ingeo Resin**	**ASTM Method**
Specific Gravity, g/cc	1.24	D792
MFR, g/10 min[2]	6	D1238
Relative Viscosity[3]	4.0	D5225
Clarity	Transparent	-
Peak Melt Temperature, °C	145-160	D3418
Glass Transition Temperature, °C	55-60	D3418
Mechanical Property		
Tensile Yield Strength, psi (MPa)	8700 (60)	D882
Tensile Strength at Break, psi (MPa)	7700 (53)	D882
Tensile Modulus, psi (MPa)	524,000 (3.6)	D882
Tensile Elongation, %	6	D882
Notched Izod Impact, ft-lb/in (J/m)	0.3 (16)	D256
Flexural Strength, psi (MPa)	12,000 (83)	D790
Flexural Modulus, psi (MPa)	555,000 (3.8)	D790
Heat Distortion Temperature, °C 66 psi (0.45 MPa)	55	E2092

1.1.4 Extrusion of Polymers

Extrusion is a fundamental shaping process used for various materials such as metals, ceramics and polymers [6]. Fundamentally, this is a compressive forming process which forces molten material through an orifice or "die" to produce a continuous and constant cross-section product or "extrudate". For polymers, various thermoplastics can be used to manufacture the desired product depending on the die used. For solid-core filaments, a simple circular die is used with a precisely machine hole. As the filament is extruded, a simultaneous drawing process is utilized by means of a spool to collect the material for later distribution. Below, the viscosity of various thermoplastics versus temperature is shown. Viscosity is a property of any fluid which relates the shear stress to the shear rate [6]. Due to the high molecular weight of polymers, when in a molten state, their viscosity is very high, as shown in Figure 3 and 4. They exhibit properties of a non-Newtonian fluid known as a "pseudoplastic fluid". For Newtonian fluids, such as water or oil, the viscosity is a constant at a given temperature. However, for a pseudoplastic fluid the viscosity is inversely proportional to the shear rate. Therefore, at higher rates of shear stress the fluid becomes much thinner. In addition to this, the viscosity of the polymer decreases with an increase in temperature. Both parameters are crucial to determine the optimal extrusion operation which lead to the highest dimensional tolerance of the final filament.

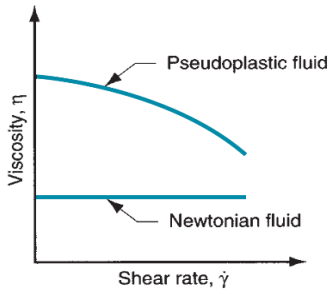

Figure 3. Viscosity relationship for Newtonian versus typical polymer melt. [6]

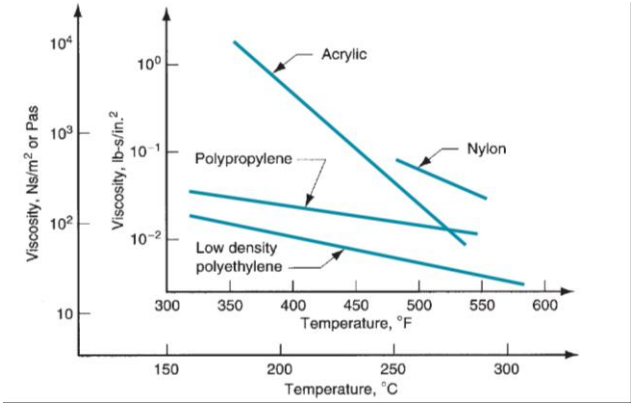

Figure 4. Viscosity versus temperature for common thermoplastics. [6]

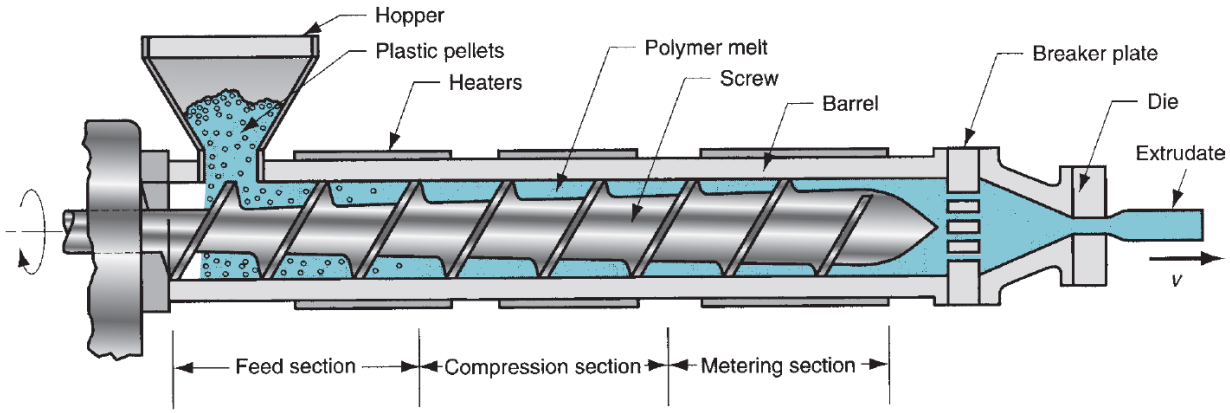

Figure 5. Schematic of a simple single-screw extruder. [6]

Additionally, a simple schematic of a single-screw extruder is shown above with major components annotated. For polymer extrusion, feedstock in the form of pellets or powder is added to the hopper and is gravity-fed to the rotating auger screw. The hopper base is interfaced with an opening in the machined barrel and the feedstock is translated further into the barrel from the rotation of the screw. The barrels are heated using induction style coils or heating cartridges which are wrapped in insulation to maintain the desired set temperature. J-type thermocouples are commonly used to measure the temperature and maintain a set point using a standard digital PID temperature controller. As the polymer is translated further along the barrel, it reaches a completely molten state known as a "polymer melt". At this stage, the melted polymer exhibits pseudoplasticity which once again shows that at high rates of shear stress the viscosity decreases. This is a beneficial phenomenon as the polymer melt experiences high shear stress due to the high flow rate and relatively small areas within the barrel and die. However, this requires a large amount of back pressure as supplied by the screw which in turn requires a high-torque motor to provide the rotation. The below schematic shows a section of the barrel and screw interface with required design parameters.

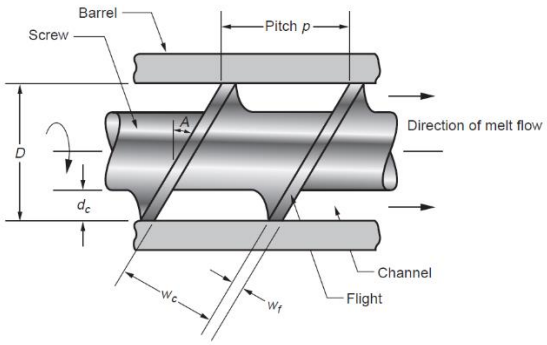

Figure 6. Schematic of a barrel and screw section. [6]

1.1.5 Newtonian Fluid

$$\tau = \eta\dot{\gamma} \tag{1}$$

1.1.6 Pseudoplastic Fluid

$$\tau = k(\dot{\gamma})^n \tag{2}$$

In the above equations, τ represents the shear stress, η represents the viscosity, $\dot{\gamma}$ represents the shear rate, k represents a constant that corresponds to the viscosity, and n represents the flow behaviour index which is less than one for a given polymer melt.

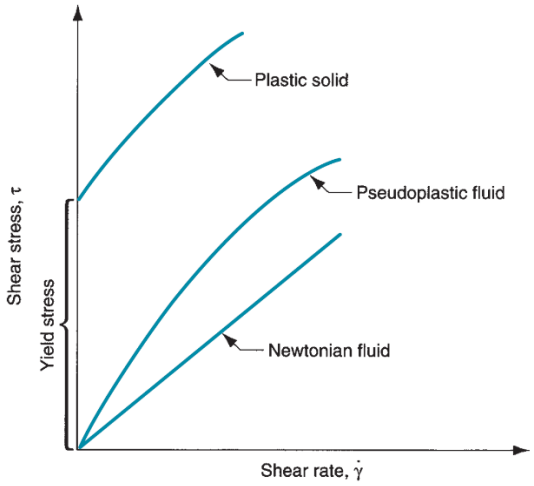

Figure 7. Viscosity behaviours of pseudoplastic versus Newtonian fluids. [6]

1.1.7 Viscoelasticity

$$\sigma(t) = E(t)\epsilon \tag{3}$$

In addition to pseudoplasticity, polymer melts demonstrate a second behavioral phenomena known as "viscoelasticity". Viscoelasticity is the property of the polymer melt that relates the strain experienced for a given stress and temperature over a given time period. It combines the viscous and elastic effects of the material and can explain some key properties of the material. In a viscoelastic solid, the stress-strain relationship is time dependent as shown in Eq (3) which is derived from Hooke's Law. $\sigma(t)$ is the stress, $E(t)$ is the viscoelastic modulus and ϵ is the strain. It can be concluded that the material behaves very differently depending on the strain rate experienced.

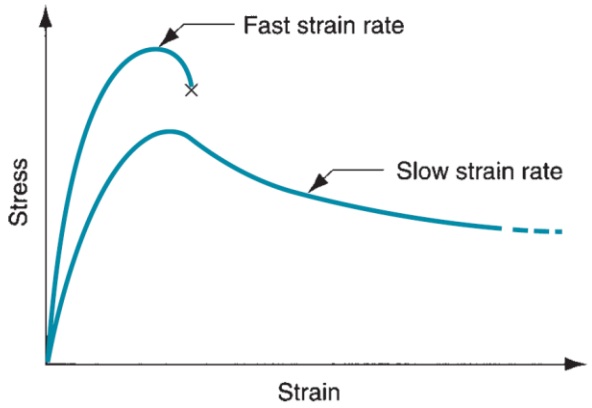

Figure 8. Basic stress-strain curve of viscoelastic material. [6]

Above, the effect of the strain rate for a viscoelastic material can be clearly seen. At a high or "fast" strain rate, the thermoplastic behaves such that of a brittle material as seen by the corresponding stress-strain curve. In contrast, for low or "slow" strain rates, the thermoplastic behaves as a viscous or elastic material. This is a very complex phenomenon; however, significant insight can be deduced from these relationships. The strain rate directly affects how the material will behave during the extrusion process. For example, an important outcome of this behaviour is a phenomenon known as "die swell". Below, the die swell phenomenon is visualized showing the extrudate expanding once it has exited the die orifice.

1.1.8 Die Swell

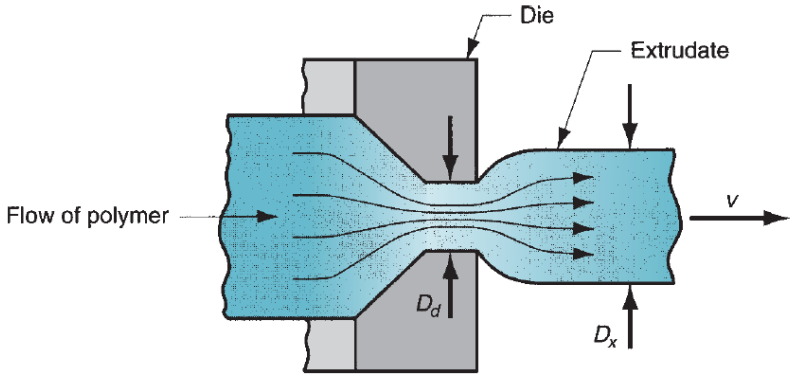

Figure 9. Die swell phenomenon. [6]

This behaviour is attributed to the shape memory of the polymer prior to entering the small die cross section. This is caused by unrelaxed residual stresses no longer being constricted by the compressive forces applied by the narrow die section. Once the extrudate exits the die, it is unconstrained and hence expands slightly. This can be avoided by simply increasing the length of the die channel to allow the time required for internal stresses to relax prior to exiting the die.

2.0 Methodology

The work was conducted in the Facility for Research on Aerospace Materials and Engineered Structures (FRAMES) in the engineering building at Ryerson University. A novel recycling process was developed at McGill University to reclaim glass fiber from the landfilled composites of end-of-use wind turbine blades. The recycling process consists of traditional mechanical grinding techniques, followed by micromechanical analysis to govern design parameters and lastly a multi-stage sieve process with a 60 μm mesh size [7]. Once the fibers are recovered and sieved to the desired fiber length, the chopped glass fiber is combined with thermoplastic polylactic acid (PLA) pellets in a twin-screw pelletizer. This process produces recycled composite pellets that can be used for various polymer forming techniques including compression molding and 3D printing. Traditional fused filament fabrication (FFF) 3D printing requires a filament feedstock material to operate. The composite pellets produced by the first extrusion process must go through a second extrusion process to transform the pellets into a solid core filament. In order to manufacture this filament to a high degree of dimensional accuracy, a single-screw extrusion system was developed in FRAMES.

2.1 Development of a Single-Screw Polymer Extrusion System

2.1.1 Desktop Extrusion Systems

As desktop-style FFF 3D printers have gained widespread use outside of the engineering industry, several companies have attempted to develop desktop-style extrusion systems. The purpose of these machines is to manufacture 3D printing filament from a lab or even a home setting. However, these systems have suffered from high cost and produce lower quality filaments compared to filament spools available from companies. Nonetheless, the hardware can be utilized in a laboratory setting and modified to improve the dimensional tolerance. Currently, the industry standard tolerance has been set at 1.75 mm$\pm$0.05 or a filament diameter variation of just 100 microns. Other manufacturers have recently claimed to have dimensional tolerance of just 30 microns. To maintain such a tight tolerance, active cooling and feedback control is essential to maintain filament accuracy. If the filament is not dimensionally accurate, the corresponding 3D prints can have defects inadvertently induced. Two candidate extrusion systems that were available in FRAMES were assessed, tested and a subsequent design began to improve the selected system.

The two extrusion systems at FRAMES were tested and benchmarked using *Ingeo* 4043D PLA. The *FilaFab* PRO 350 EX was selected as it has a variable and overall higher RPM capability compared to the *Noztek* system.

Figure 10. *FilaFab* PRO 350 EX and filament winder. [8]

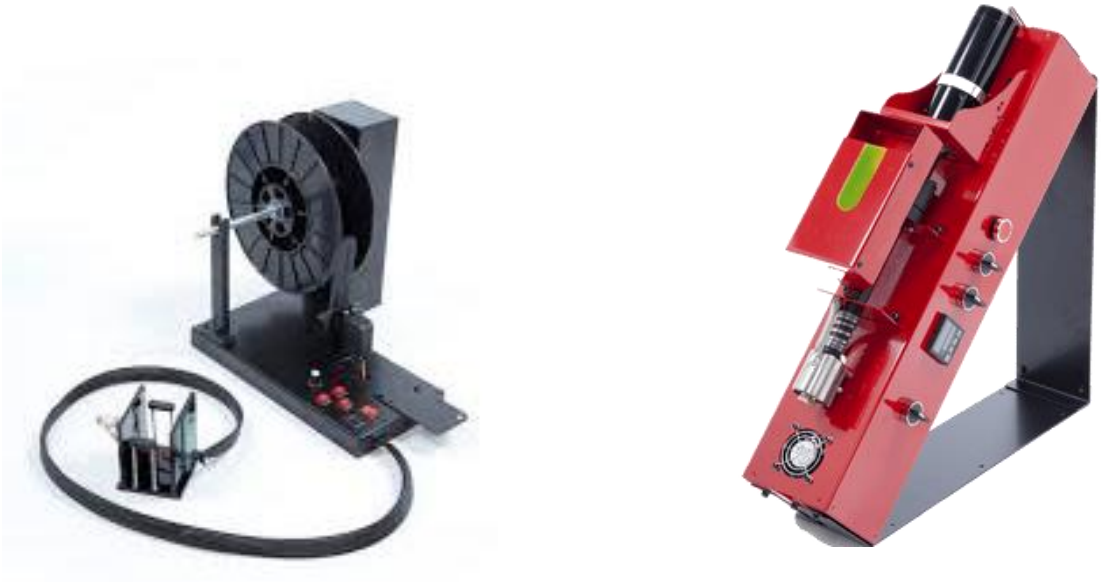

Figure 11. *Noztek* Pro high temperature extruder and filament winder. [9]

Although the maximum operational temperature of the *FilaFab* is around half that of the *Noztek*, the system was found to perform better for long duration extrusion trials. An extruded aluminum frame was designed in CATIA V5 and assembled to form the frame of the extrusion system. Once the *FilaFab* extruder and winder were interfaced, peripheral cooling and feedback control systems were designed and implemented. The primary feedback control sensor was the *Keyence LS9030M* laser micrometer which was used to actively monitor and control the filament diameter [10]. Furthermore, a radial air-cooling adapter was designed and 3D printed using a digital light projector (DLP) resin printer to accommodate the complex inner geometry. This adjustable air cooler was placed near the exit of the die to immediately cool the filament as it exited the die to maintain the diameter and increase manufacturing speed.

2.1.2 Our Extrusion System

To begin, Figure 12 and 13 show the CATIA V5 design compared to the actual extrusion system developed based on the FilaFab PRO 350 EX extrusion platform. Custom peripheral controls were designed and interfaced to maintain dimensional accuracy throughout trials.

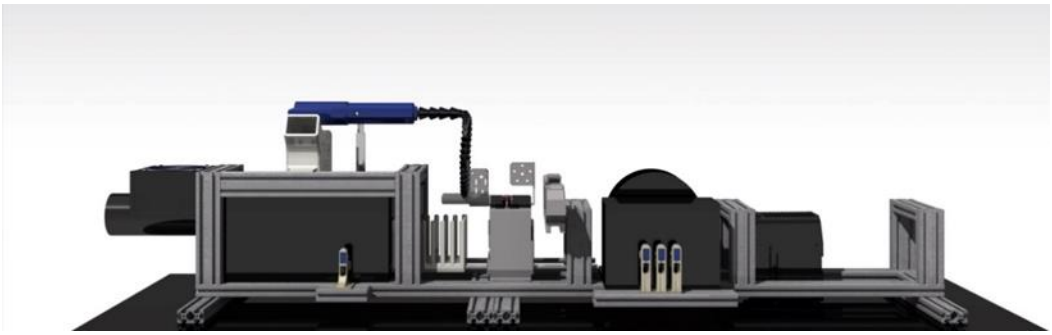

a)

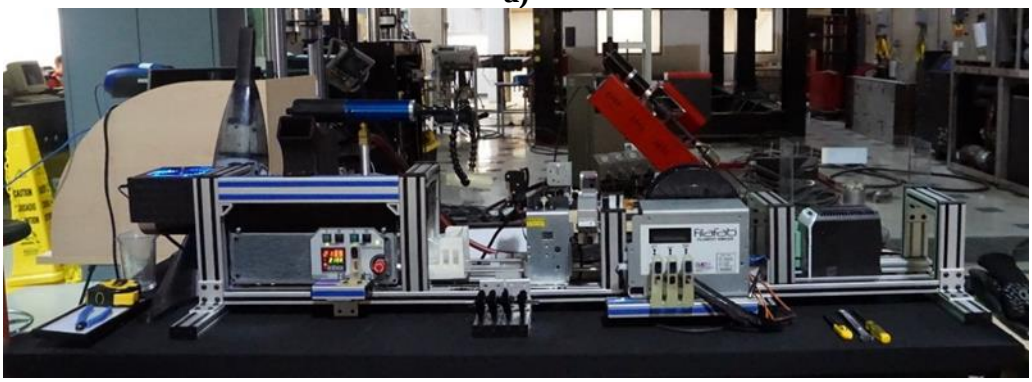

b)

Figure 12. FilaFab PRO 350 EX: (a) CATIA V5 rendering; and (b) constructed system.

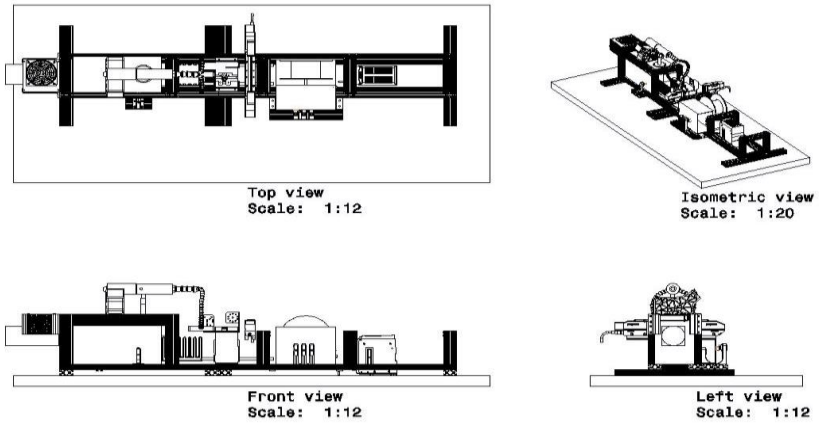

Figure 13. Basic 3-View and isometric view of system.

Figure 14 has been annotated to label the major elements of the extrusion system designed to produce high quality thermoplastic materials for 3D printing.

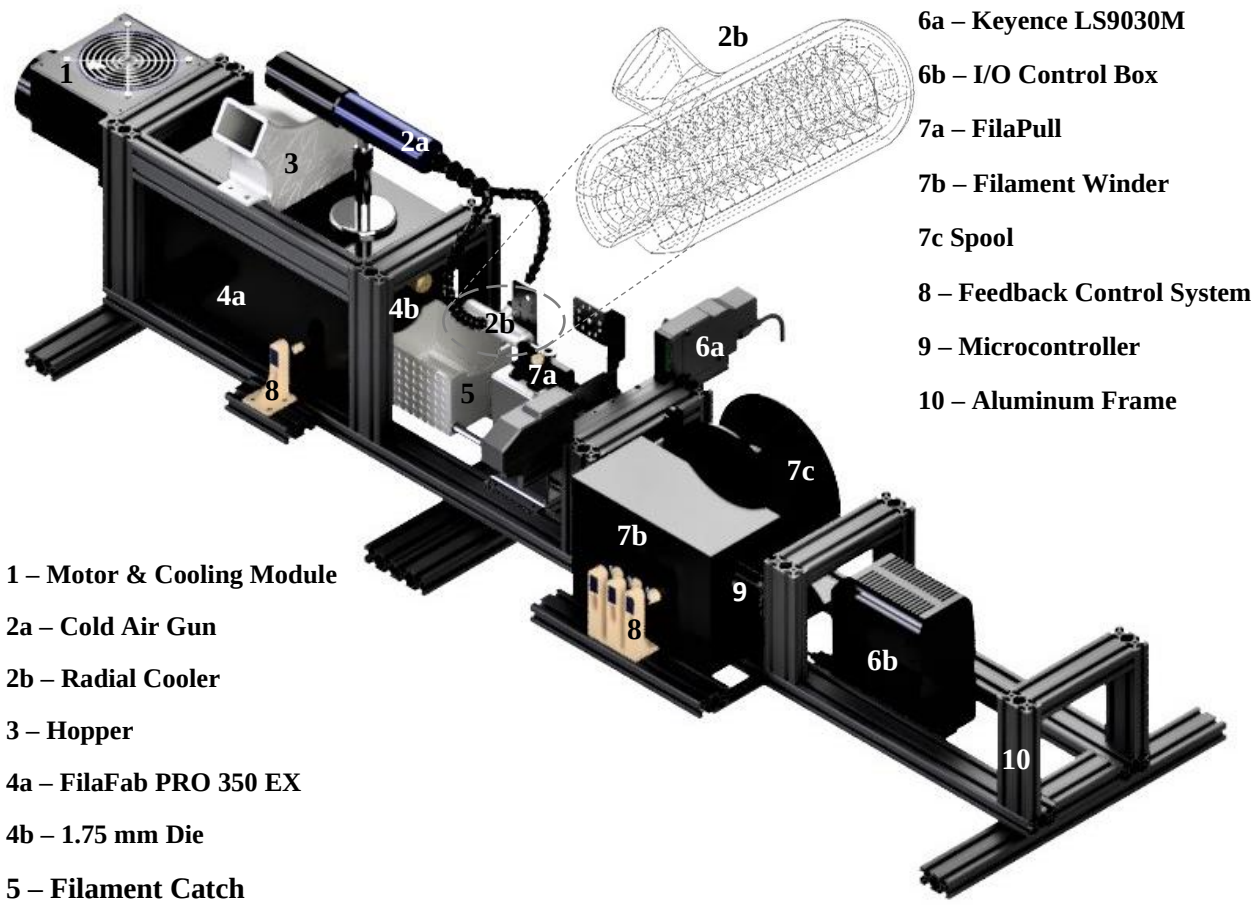

Figure 14. Overview of extrusion system.

The start up, operation and shut down procedures were created and summarized in a user manual. The next section will provide a brief overview of its operational procedure developed to produce the composite filaments.

2.1.3 Operation of the Extrusion System

Material Preparation: Dehydration

The dehydration procedure used for PLA and composite pellets consists of a 4-hour dehydration process at 60 °C. This allows the material's water content to be evaporated prior to the extrusion process to improve both the internal structure and surface finish.

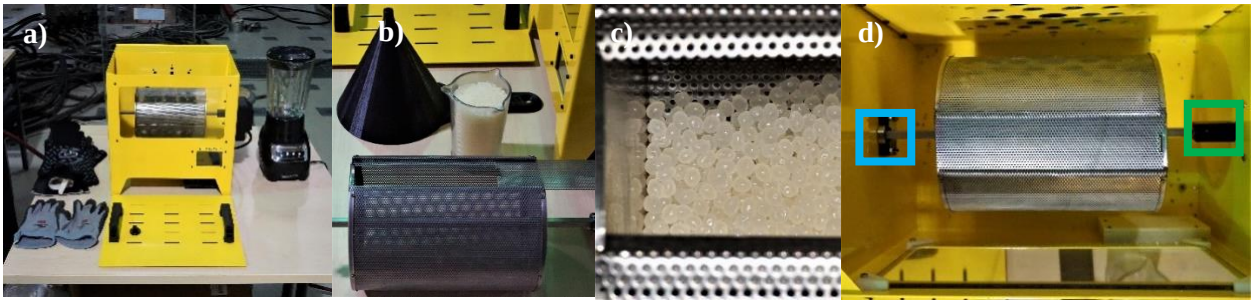

Figure 15. Dehydration: (a) dehydrator; (b) funnel; (c) drum; and (d) install drum.

Phase I: Purge

Once the system has preheated for at least 30 minutes at the required temperature, pure PLA is added to purge any material left over from a previous trial. This purged material is saved, to be ground up and re-extruded for future studies.

Figure 16. Purge: (e) fill hopper; (f) preheat; and (g) purge.

Phase II: Spool

Once filament is extruding consistently, the filament can be wound on the spool as shown. Settings must be manually adjusted at first to achieve a consistently spooled filament.

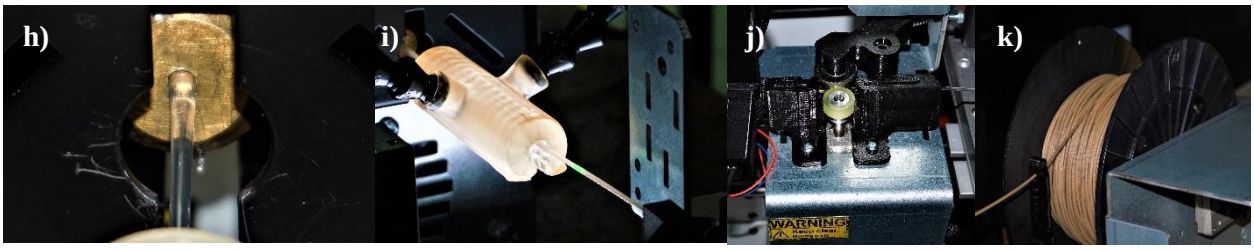

Figure 17. Spool: (h) 1.75 mm die; (i) cooling; (j) drawing; and (k) spooling.

Phase III: Feedback Control

Lastly the feedback control system can be activated using the software package previously developed by another undergraduate research assistant at FRAMES, Mr. Samuel Woolsey. This software actively monitors and adjusts the system if necessary while recording the filament diameter data.

Figure 18. Feedback: (l) I/O box; (m) extruder; (n) winder; and (o) initialize software package.

Figure 19 provides an overview for the flow of information to provide feedback control for the extrusion system.

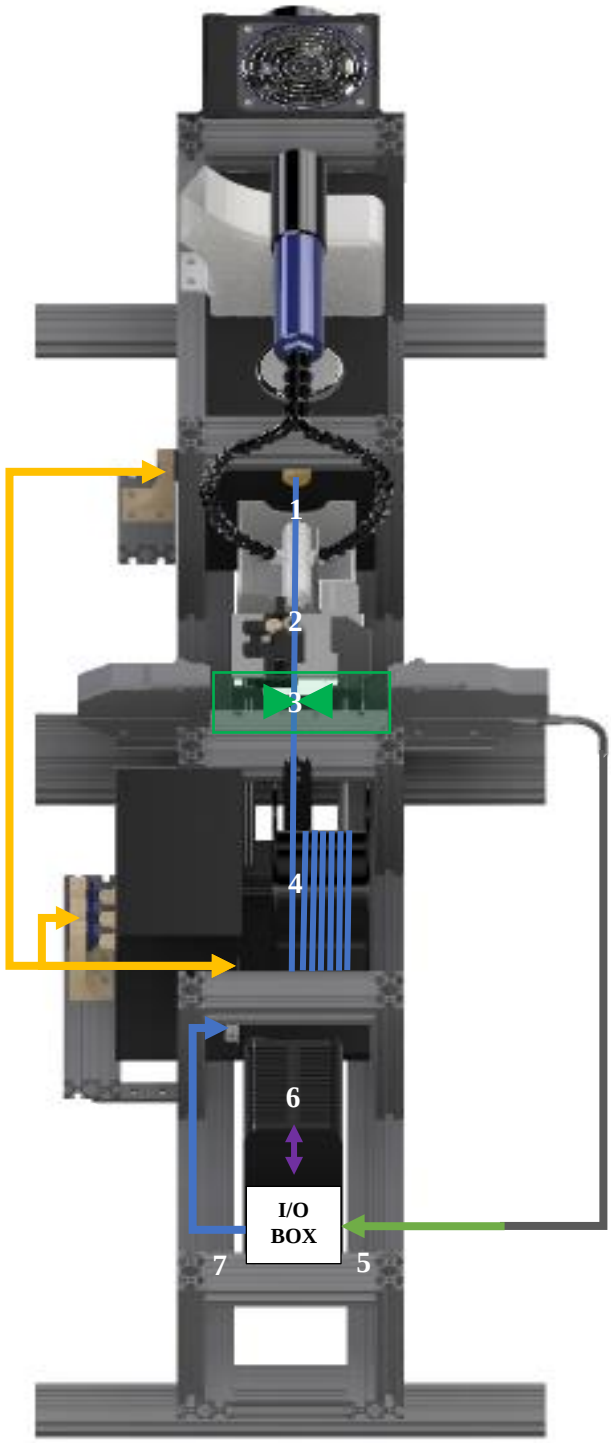

1 – 1.75±0.05 mm Extrudate

2 – FilaPull Drawing Mechanism

3 – LS9030M Laser Micrometer Measurement

4 – Filament Wound on the Spool

5 – Input from Micrometer into I/O Box

6 – I/O Box and Computer Software

7 – Output to the Arduino Microcontroller

8 – Winder Feedback Control Hardware

9 – Extruder Control Hardware

The annotations highlight the key flow of information as the extrudate (1) exits the die, is drawn by the rollers located at (2), the diameter measured at (3), drawn and spooled at (4), the information transfer to the I/O box (5), the interfacing with a laptop computer and custom feedback control software (6), the output to the microcontroller (7) and lastly to the direct control of the system's extrusion parameters via the designed servo controls (8 & 9).

The control software actively monitors the filament diameter and makes decisions using PID control theory. The data is measured throughout the trial to improve the control software's accuracy. The system can be operated in manual, semi-automatic and automatic modes throughout an extrusion trial.

Figure 19. Feedback control architecture.

2.1.4 Final Extrusion System

To conclude, Figure 20 shows the final design and configuration of the extrusion system developed to manufacture advanced materials for use in additive manufacturing applications.

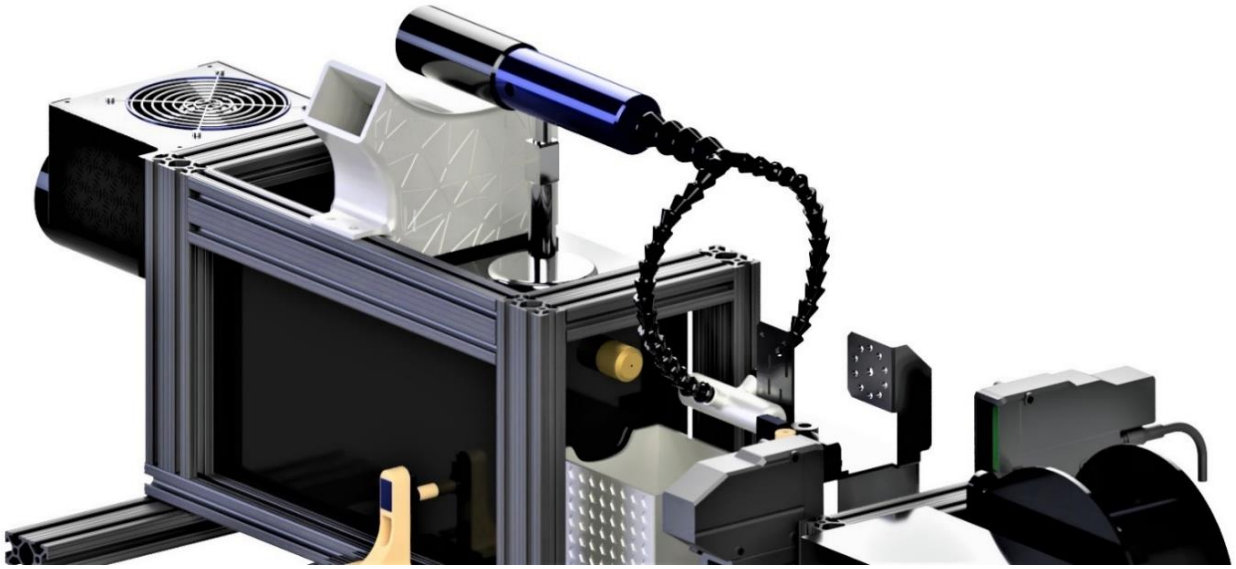

a)

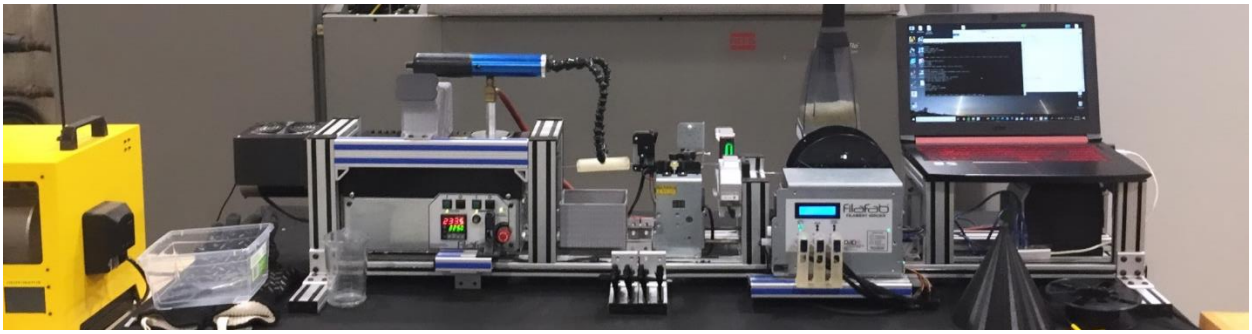

b)

Figure 20. Final extrusion system: (a) rendered; and (b) actual.

This system is capable of extruding thermoplastic polymers with a variety of additives to achieve a desired material characteristic. The current maximum operating temperature is 250 °C. However, the system is compatible with the *Noztek HT* extruder which can reach a maximum temperature of 600 °C. The system is therefore extremely versatile with the ability to extrude high performance thermoplastics such as fiber-reinforced nylon, polycarbonate (PC), polyether ether ketone (PEEK), and other materials. Paired with the available 3D printers and tensile test machines, rapid development of next-generation materials is feasible.

2.2 Recycling Fiberglass from Landfilled Wind Turbines

2.2.1 Overview of the Procedure

This section aims at presenting the summary of the filament manufacturing and the production of the ASTM D638-14 coupons printed with a raster angle of 0° for each of the 24 plies or simply denoted as $[0]_{24}$. With the process presented previously, the 3%, 5% and 10% by weight recycled fiberglass reinforced PLA pellets can be dehydrated and extruded to produce spools. Once these spools are manufactured, they can be used on a modified Prusa Mk2 i3 FFF 3D printer to create coupons. The 3D printer's nozzle and hotend was upgraded to allow for the printing of the critical fiber length composite, free of jams or feeding issues. The coupons were weighed, labeled and scanned before being shipped to McGill University for tensile testing and SEM imaging. The work completed during Winter 2020 semester was only a part of a larger project on recycling wind turbine blades. Previous works first investigated the proof of concept with a comparison between pure PLA coupons and 5% by weight recycled fiber glass reinforced PLA [7], next the study of varying the fiber percentage in addition to the use of virgin fibers was compared [11], and now the focus of this thesis is on the critical fiber length. Figure 21 shows the overview of the recycling and manufacturing process used to create and test coupons.

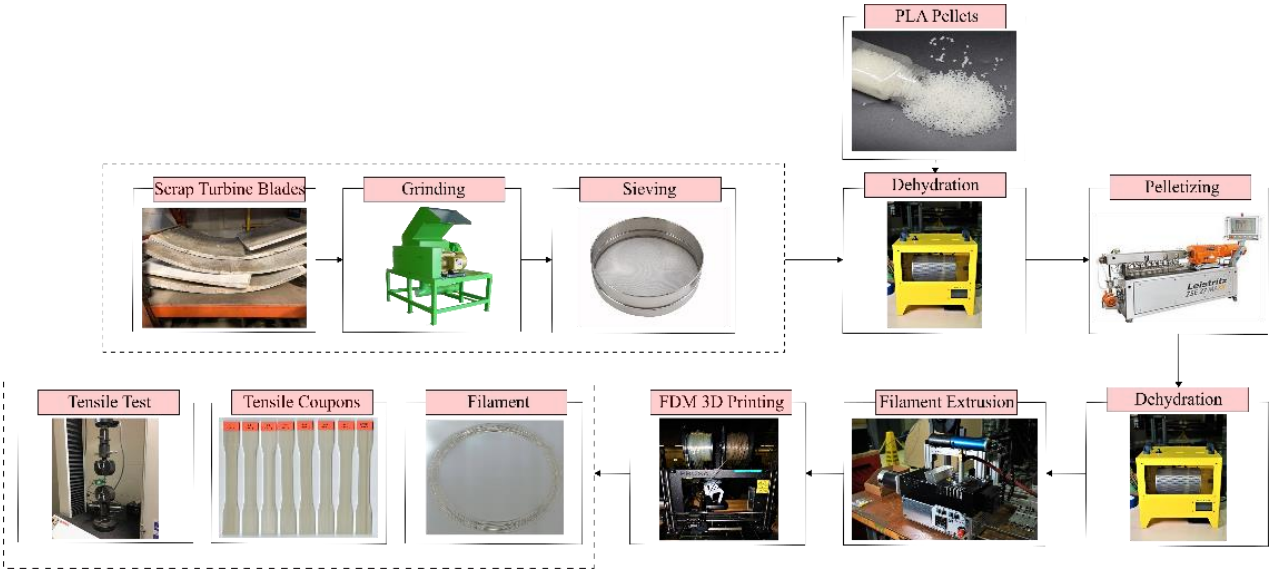

Figure 21. Overview of the recycling and coupon manufacturing process. [7]

Furthermore, Figure 22 shows the major steps required to manufacture the recycled composite feedstock to produce the filament needed to manufacture the coupons using 3D printing.

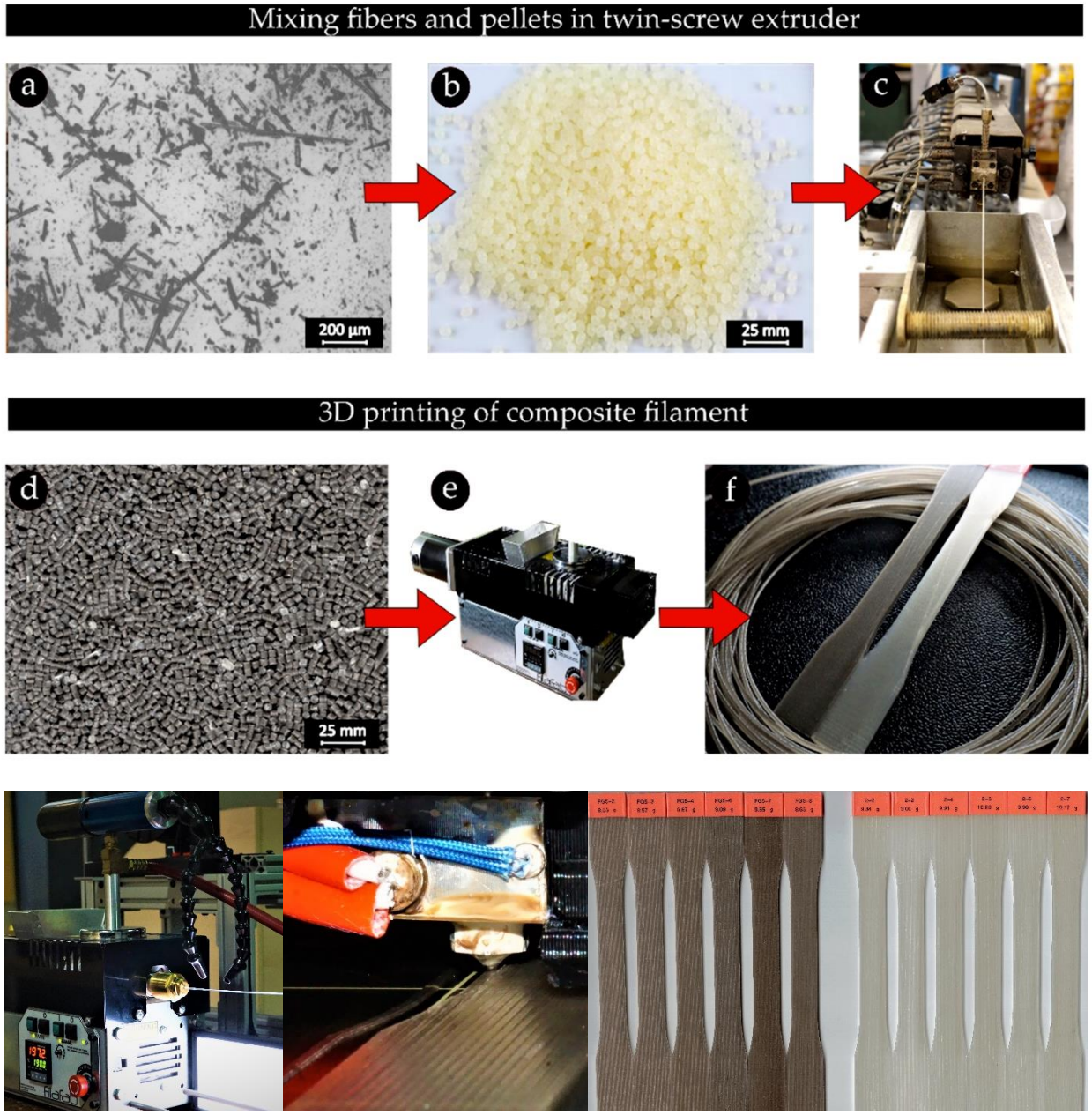

Figure 22. (a) fibers; (b) PLA pellets; (c) pelletizer; (d) RFG pellets; (e) extruder; and (f) coupons. [7]

The annotations represent the process as follows: a) recycled fibers are incorporated with b) PLA in a c) twin-screw pelletizer to produce d) recycled composite pellets which are extruded using a e) single-screw extruder and manufactured into f) coupons via 3D printing. Since short fibers were used for this study, a standard 0.4 mm brass nozzle was used as indicated by the fine unidirectional beads.

Figure 23 shows the coupons with increasing fiberglass percentage by weight increasing from 0 wt% to 25 wt% from left to right as shown.

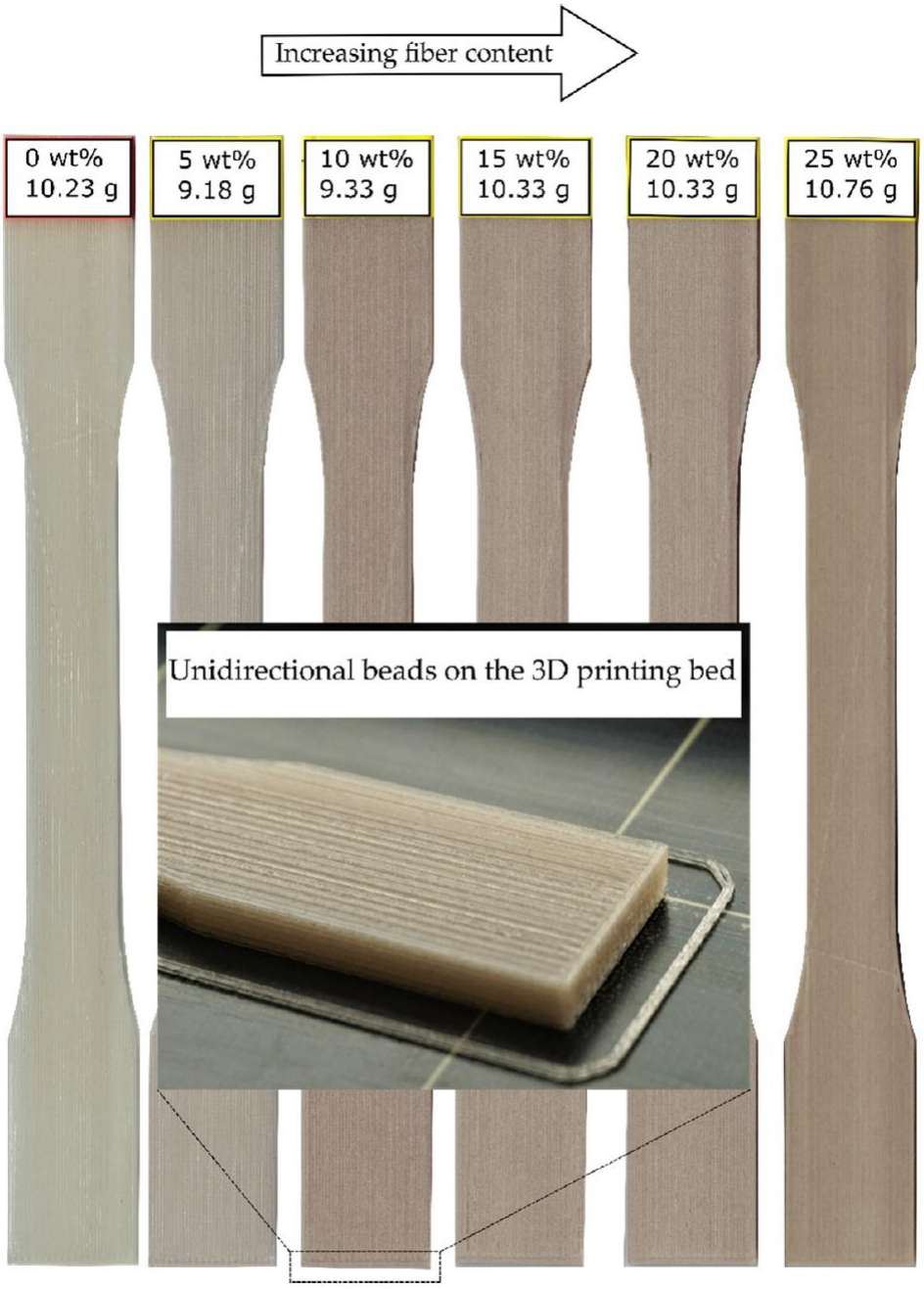

Figure 23. Coupons with varying fiber content by weight. [11]

A visible darkening of the coupon appearance is seen as the fiber content is increased, with 25 wt% appearing the darkest out of the six specimens.

SEM micrographs are conducted to show the reinforced glass fiber within the composite filaments manufactured with varying percentages of chopped fibers.

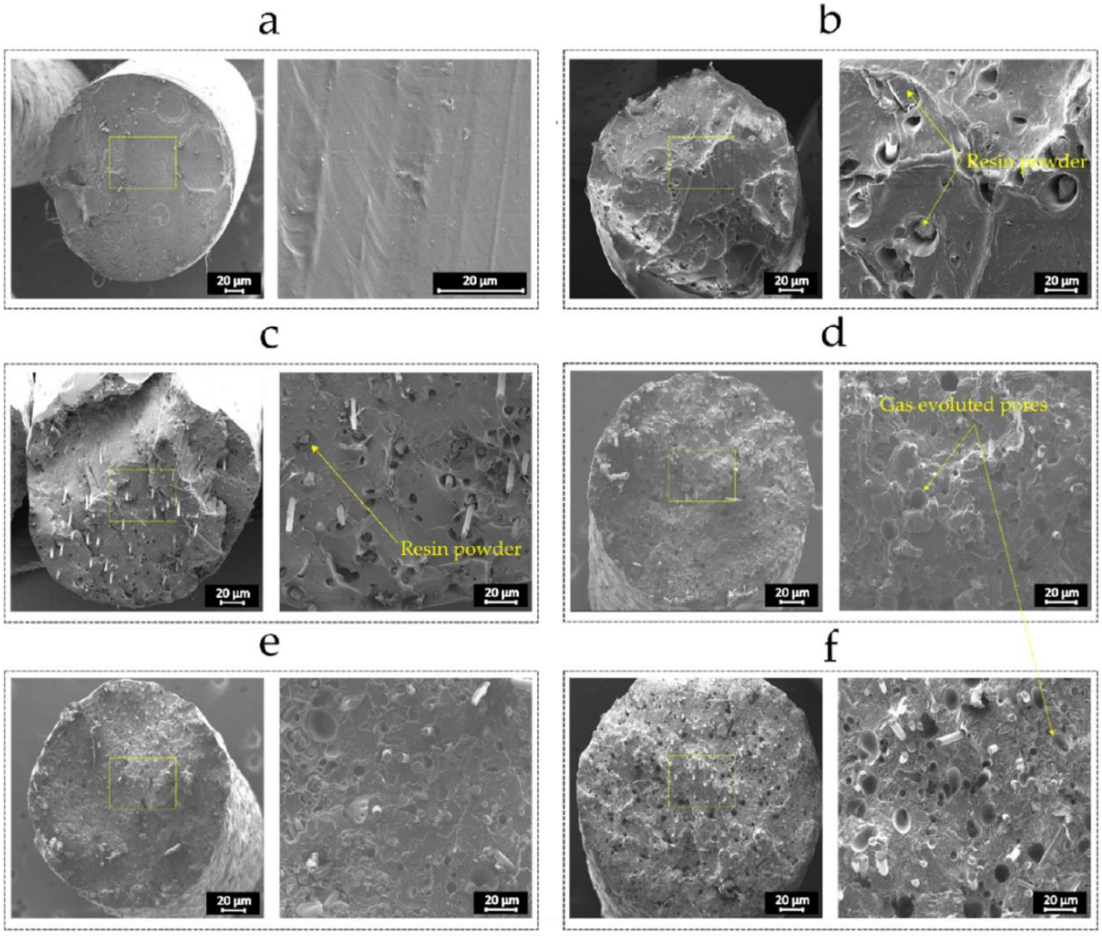

Figure 24. SEM1 (a) PLA (0%); (b) 5% wt; (c) 10% wt; (d) 15% wt; (e) 20% wt; and (f) 25% wt. [11]

SEM images were taken of the filament cross-section for each material manufactured as follows: a) Pure PLA (0% wt), b) 5% wt, c) 10% wt, d) 15% wt, e) 20% wt, and f) 25% wt. The glass fibers are clearly visible as they protrude out of the cross-sections. The relative density of the fibers can be seen to increase with the increase in fiber content by weight. Left over resin powder from the recycling process in addition to gas pores have been annotated. These micrographs show that a large amount of the fibers are in-line with the filament even though the chopped fiber was randomly mixed. A potential explanation for this quality comes from the nature of the extrusion processes experienced. As previously mentioned, pseudoplastic fluids exhibit viscoelastic behavior meaning their viscosity is directly affected by shear stresses. Within the confined flow, a no-slip condition exists at the wall of the barrel which forms a characteristic parabolic velocity profile with the peak located at the centerline. The decreased viscosity at the walls due to the increased shear stress combined with the velocity profile, appear to align the fibers throughout the filament.

SEM micrographs are conducted to show the reinforced glass fiber within the composite coupons manufactured with varying percentages of chopped fibers, at the failure cross-section.

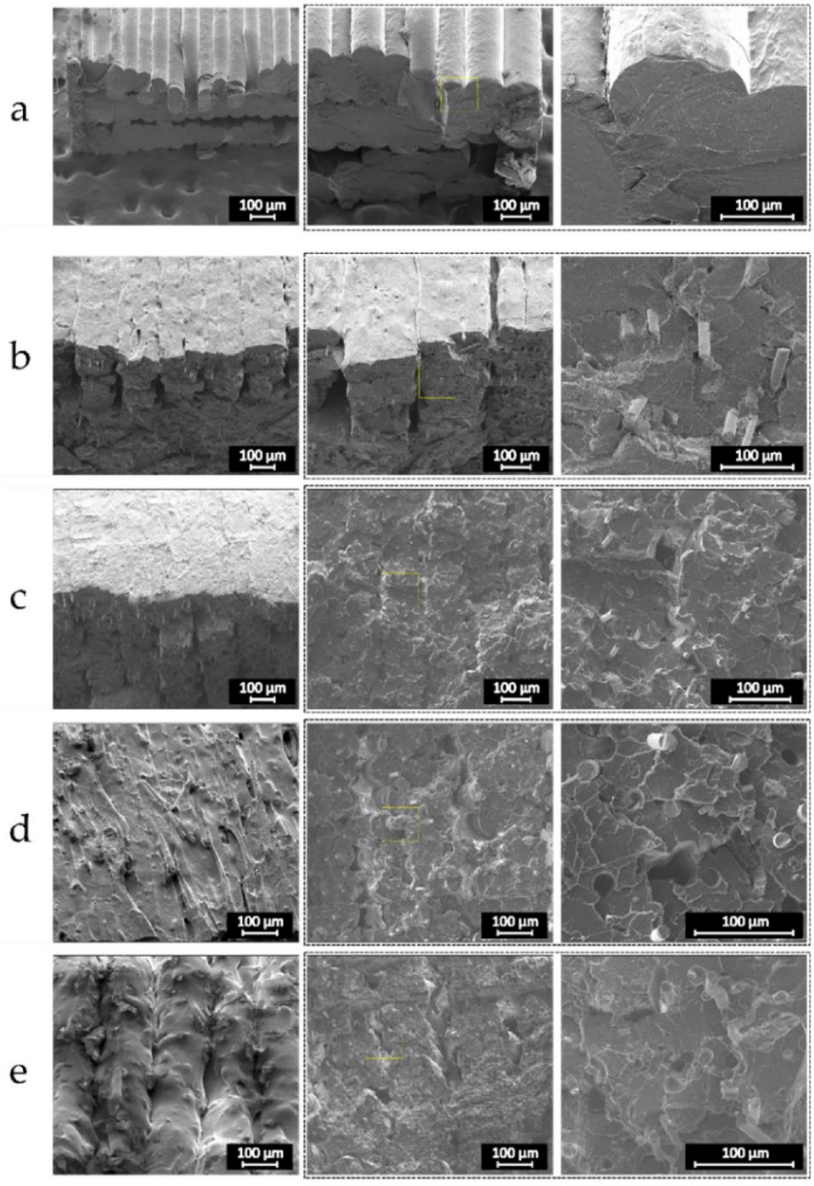

Figure 25. SEM2 (a) PLA (0%); (b) 10% wt; (c) 15% wt; (d) 20% wt; and (e) 25% wt. [11]

SEM images were taken of the fracture cross-section for the coupons tested. The labels correspond to the materials as follows: a) Pure PLA (0% wt), b) 10% wt, c) 15% wt, d) 20% wt, and e) 25% wt. Each bead shown here is approximately 0.4 mm due to the nozzle size. The beads of the coupons for this current study are three times as wide with the same height of 0.14 mm.

In Figure 26, the stress-strain curve for each of the materials is shown. To draw conclusions of the material characteristics, the stress-strain curve of each material must be produced and analyzed.

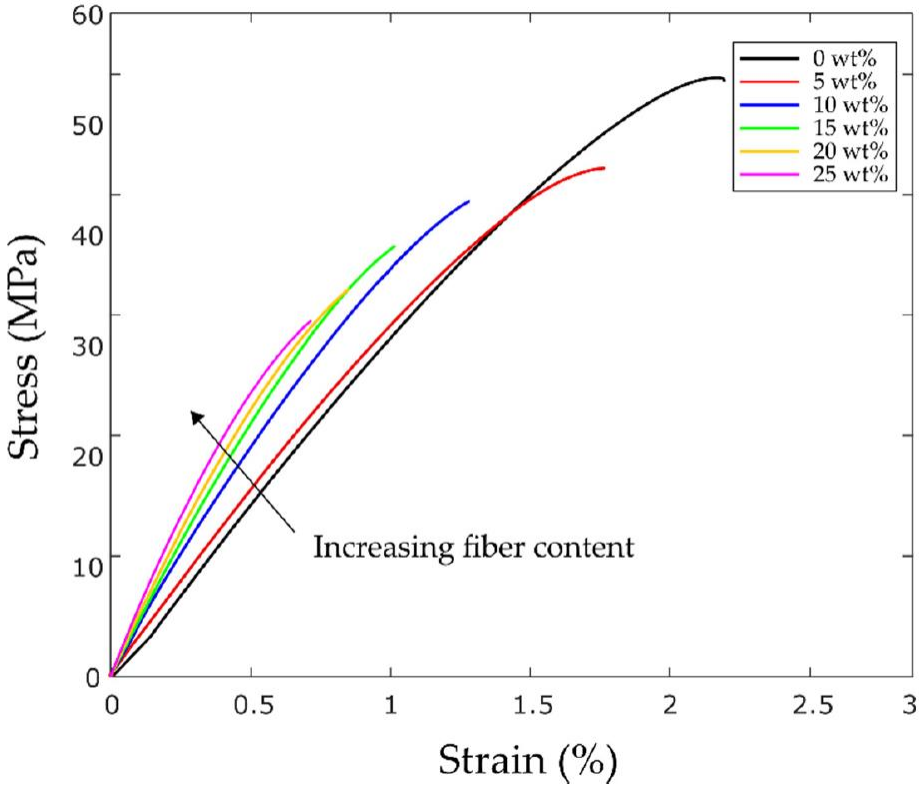

Figure 26. Stress-strain curves of D638 coupons tested with various fiber content. [11]

There is a direct correlation with the stiffness of the material and the percentage of reinforced fiberglass content found in the material. With increasing fiber content, the stiffness is also observed to be increasing. However, the strength of the materials has been negatively impacted which was partially attributed to voids induced in the coupons. The voids could have been attributed to the gas pores shown previously due to degrading epoxy resin. These voids can lead to stress concentrations which ultimately lead to early failures of the coupons during testing. Improved processing of the recycled material could improve these issues. Additionally, the short fibers may have contributed to these small defects as there are more opportunities for small pores to form at the fiber ends. To determine whether both the stiffness and strength could be improved, longer critical fibers were to be studied, which is the focus of this thesis.

2.2.2 Material Preparation

Figure 27 shows the dehydration process for each of the long fiber recycled composite pellets. This method of material preparation is essential to producing high quality filaments.

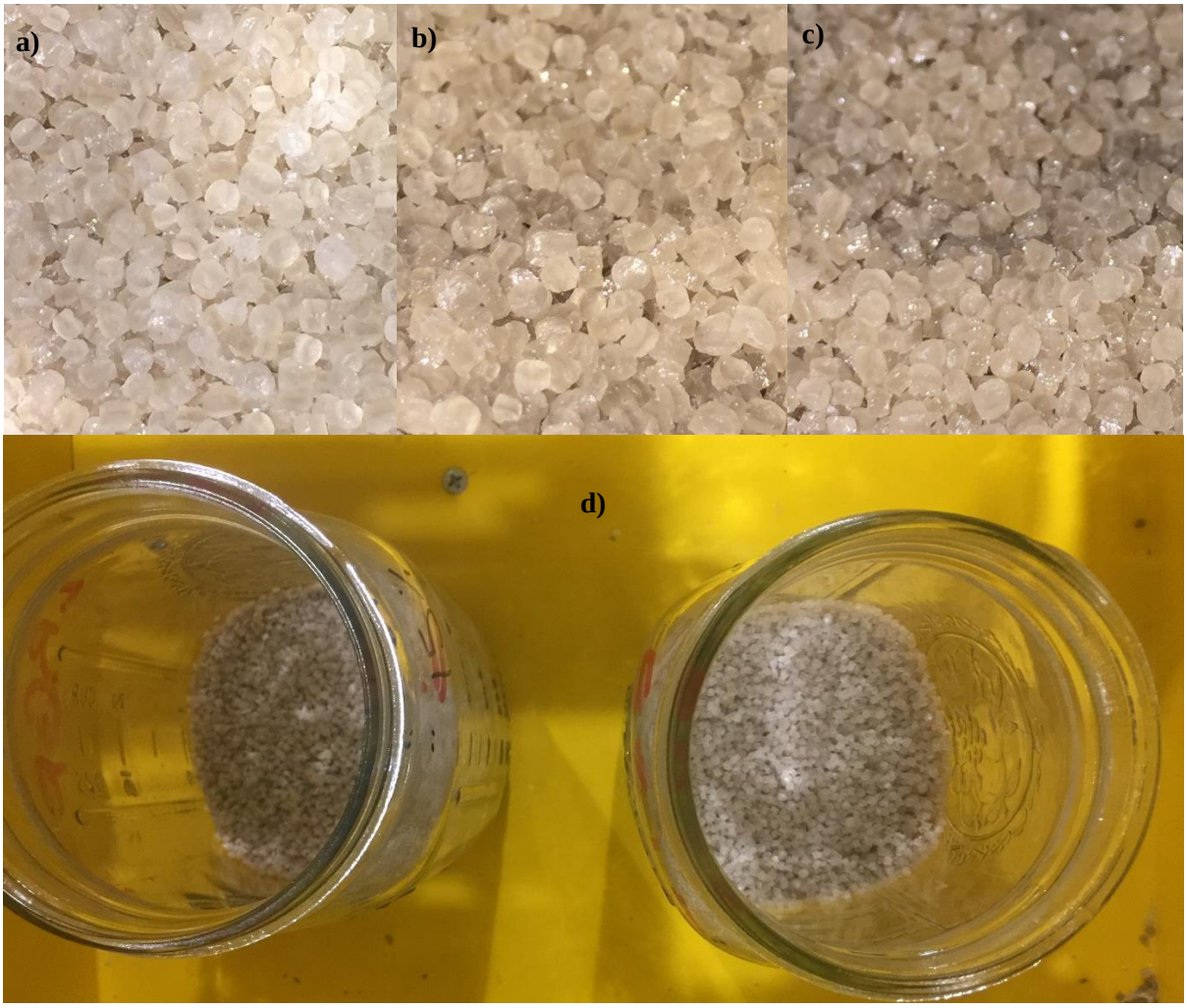

Figure 27. Preparation of: (a) 3% wt; (b) 5% wt; (c) 10% wt; and d) in dehydrator.

All the material was dehydrated for 4 hours at a temperature of 60 °C prior to the extrusion to avoid defects induced from escaping water as it is vaporized inside the barrel. Above the 3%, 5%, and 10% critical fiber-length recycled fiberglass pellets can be seen from left to right. As the fiber content increases, the colour of the pellets generally appears darker.

Figure 28 shows the dehydration for the pure PLA pellets in addition to pyrolyzed pellets to be used for a different study.

Figure 28. Preparation of: (e) PLA; (f) 3% pyro-RFG-PLA pellets; and (g) in dehydrator.

Additionally, pure PLA pellets as well as 3%, 5%, and 10% pyrolyzed recycled fiberglass pellets were dehydrated and manufactured into spools. The pyrolyzed spools are to be used for another research paper investigated the effects of burning off any remaining epoxy residue on the chopped fibers.

2.2.3 Filament Manufacturing

The system is preheated to a temperature of 215 °C and purged using pure PLA prior to extrusion. The filament must pass throught each key stage as shown in Figure 29.

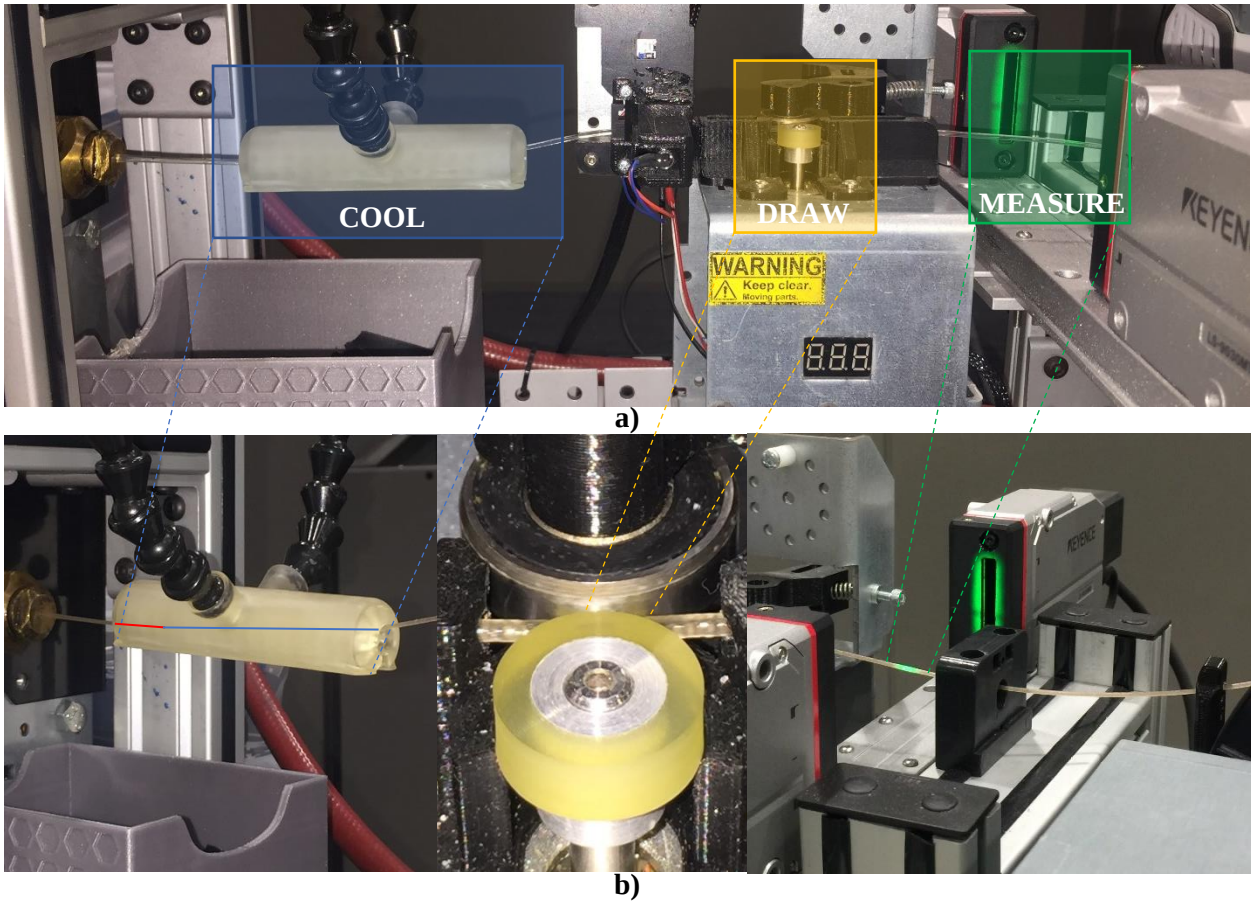

Figure 29. Filament manufacturing: (a) overview; and (b) cool, draw and measure stages shown.

Once the pure PLA is spooling neatly for approximately 15 minutes, the feedback control system can be initiated. At this point, the desired material to be manufactured is added to the hopper and sealed. The filament's appearnce should change after 15 minutes when extruding a different material from pure PLA. As shown above, the radial cooler decreases the temperature of the filament very soon after exiting the die. The radial cooler has135 small holes that completely surround the filament to rapidly cool it. It was designed to be interfaced with an exiting cold air gun with ¼" lockline hoses. It requires a supply of air throughout the trial with a gauge pressure of approximately 10 psi (~69 kPa). The FilaPull drawing mechanism uses a stepper motor with a polyeurethane roller and bearing to draw the filament. The LS9030M measures the filament diameter with a two micron accuracy using a InGaN green LED. At this point the filament is being monitored by both the user and the feedback control system. If at any point there is an issue, the feedback control system can be switch into manual operation and necessary issues can be fixed.

Each trial consisted of manufacturing 175 g of feedstock which took approximately 1 hour total in most cases. The spools shown in Figure 30 were all the required spools for this study.

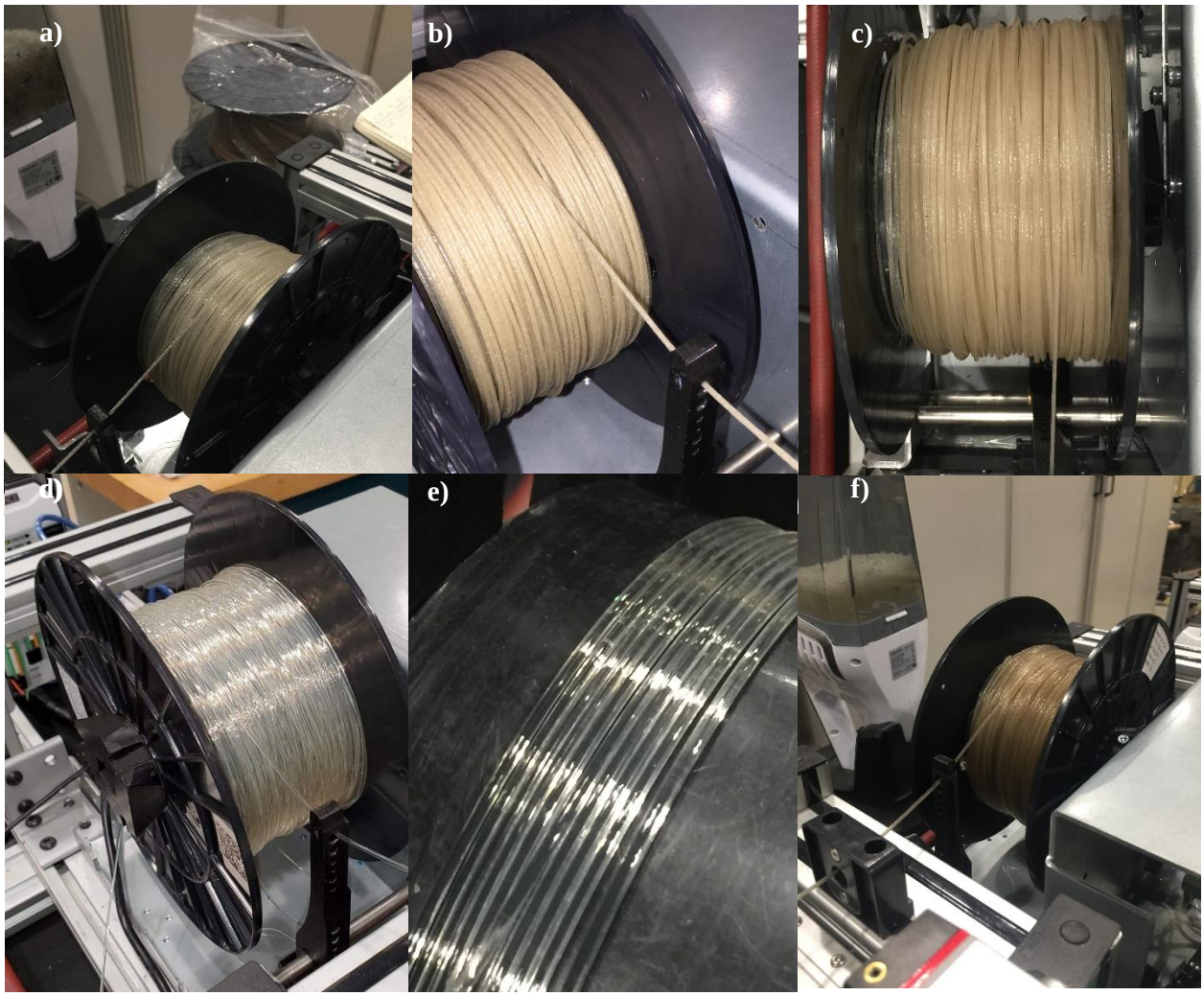

Figure 30. Manufactured spools: (a) 3%; (b) 5%; (c) 10%; (d) PLA; (e) closeup; and (f) 3% pyro.

Once the spools are complete, they are simply removed from the extrusion system and ready for 3D printing. When the material is not being used, they are stored in plastic bags with silica desiccant to prevent water absorption.

2.2.4 Prusa Mk2 i3 E3D Volcano Hotend Upgrade

To accurately and reliably print with critical fiber length composite materials, it was determined that a larger nozzle diameter was needed.

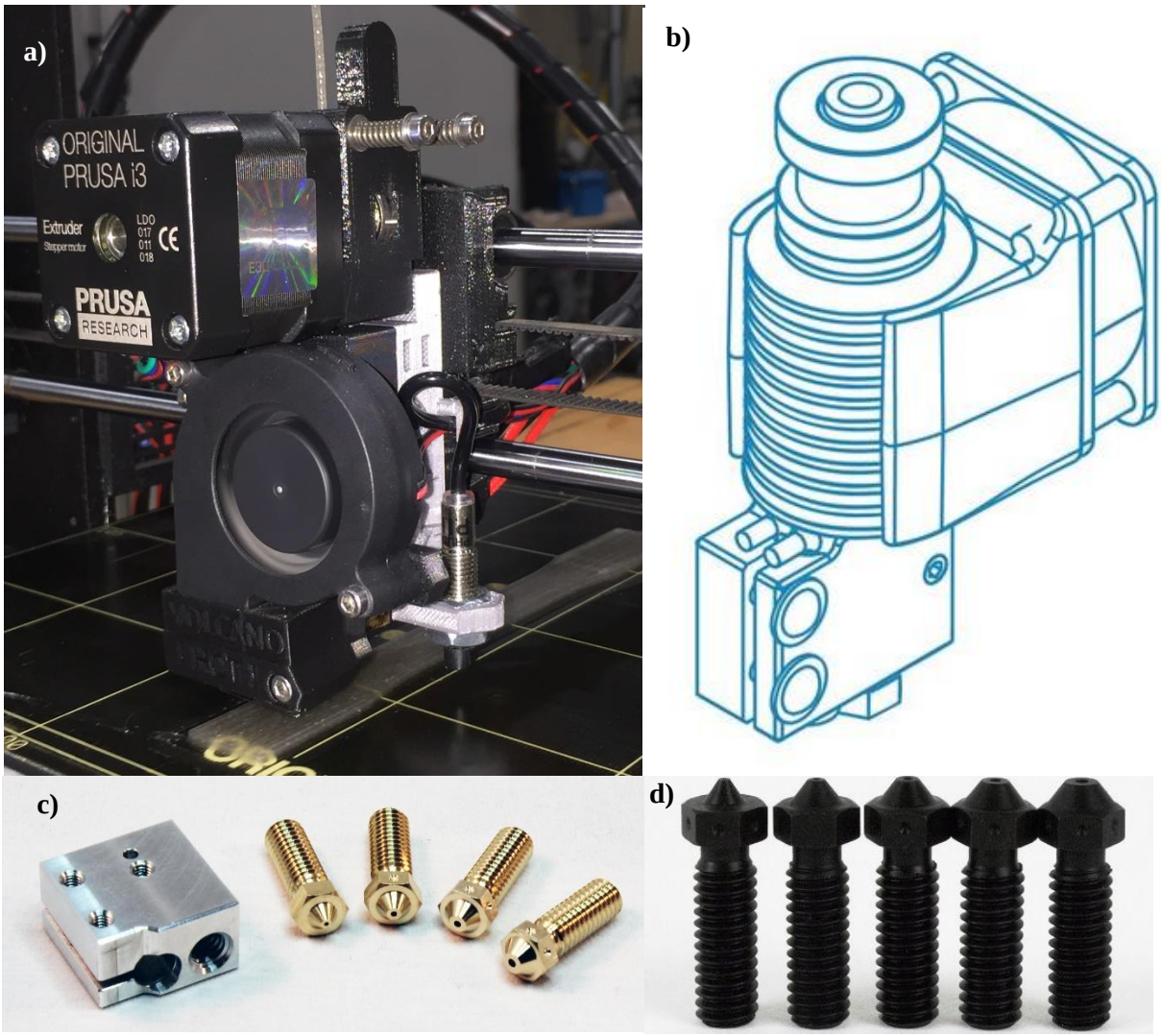

Figure 31. (a) upgraded hotend; (b) schematic; (c)heating block; and (d) steel nozzles. [12]

A complete upgrade of the existing Prusa Mk2 i3 was undertaken by using a E3D Volcano Hotend. Hardened steel nozzles were selected due to the abrasive nature of the material. A nozzle diameter of 1.2 mm, three times conventional nozzles, to accommodate for the large fibers.

2.2.5 GCODE Generation in Simplyfy3D

The simulated coupon is shown with a later height of 0.14 mm and a nozzle width of 1.2 mm. In addition, a comparison to the 0.4 mm nozzle with is shown on the top right. The bead width of the print 'fibers' and the shell is much more defined as expected for the larger nozzle.

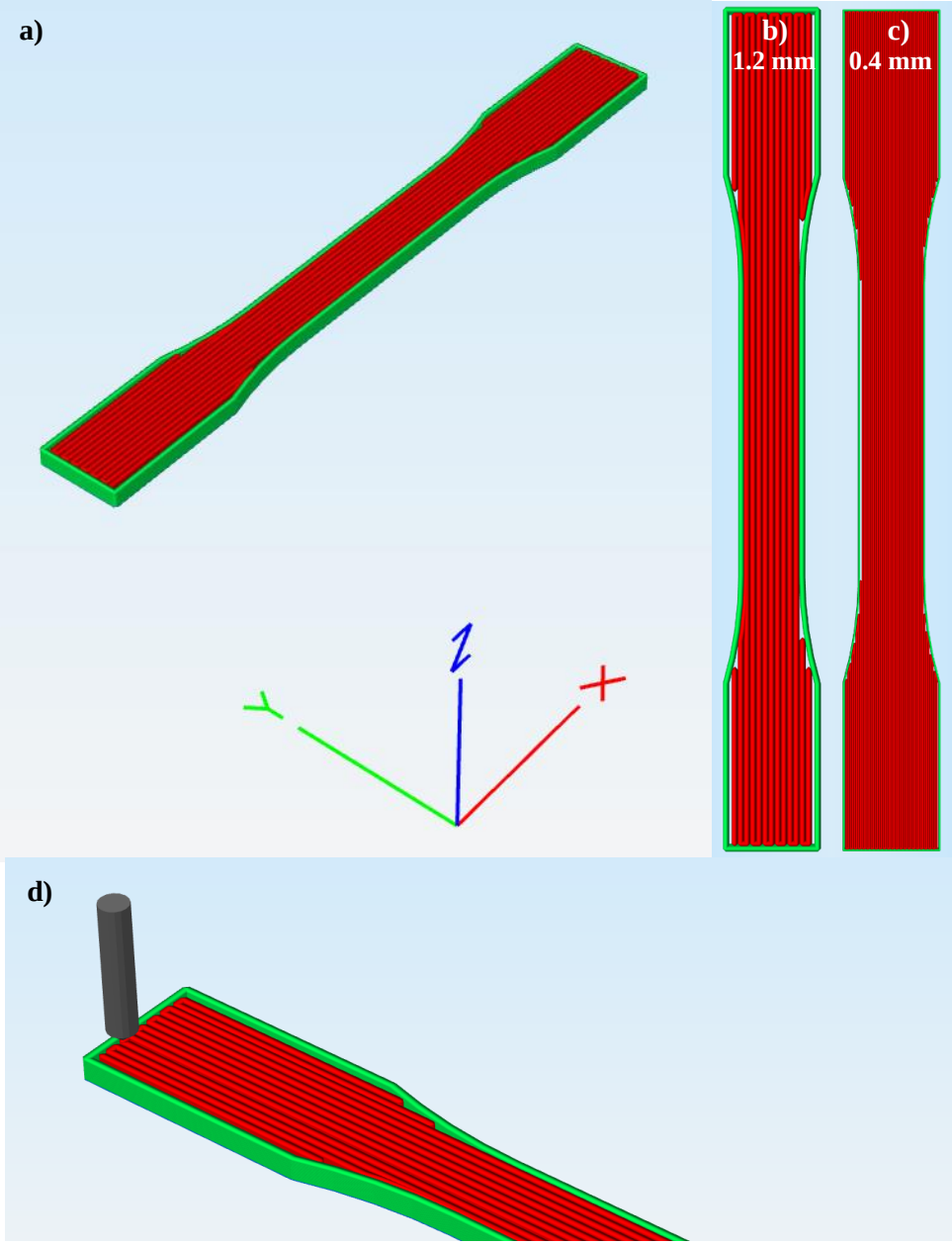

Figure 32. (a) isometric view; (b) 1.2 mm bead width; (c) 0.4 mm bead width; and (d) closeup.

The .gcode required to print the coupons was generated using a 3D printer slicer software called *Simplify3D*. For the previous works mentioned, the same slicer was used. However, with the addition of the larger nozzle size, some of the printing parameters required adjustment. To maintain the consistency with previous works, the same XYZ movement speeds and other key printing parameters were left unchanged. The only printing parameter that required a change was the extrusion width to accommodate for the 1.2 mm nozzle. Furthermore, since the inherent flowrate of the larger nozzle was much larger than the previously used 0.4 mm nozzle, the coupons were manufactured in half the time. A table has been created below to summarize the key printing parameters selected to generate the required .gcode.

Table 2. Printing parameter summary for all coupons manufactured.

Manufacturing Parameter	**Value**	**Manufacturing Parameter**	**Value**
Print Direction	XYZ	Nozzle diameter (mm)	1.2
Raster Angle	0	Nozzle temperature (°C)	215
Layer Height (mm)	0.14	Cooling	Fan Cooling
Bed Temperature (°C)	60	Infill (%)	100
Print Speed (mm/min)	2400	Filament diameter (mm)	1.75

A side view of the coupon is shown one the last of 24 layers total with a correpsonding layer height of 0.14 mm.

Figure 33. Side view of GCODE preview.

2.2.6 Coupon Manufacturing

A composite ASTM D638-14 coupon can be seen on the build plate as it is being manufactured. The filament is drawn directly into the extruder of the printing via a direct drive system. This is a necessary feature as the reinforced fiber filament is extremely stiff and could potentially snap in a Bowden-style FFF 3D printer.

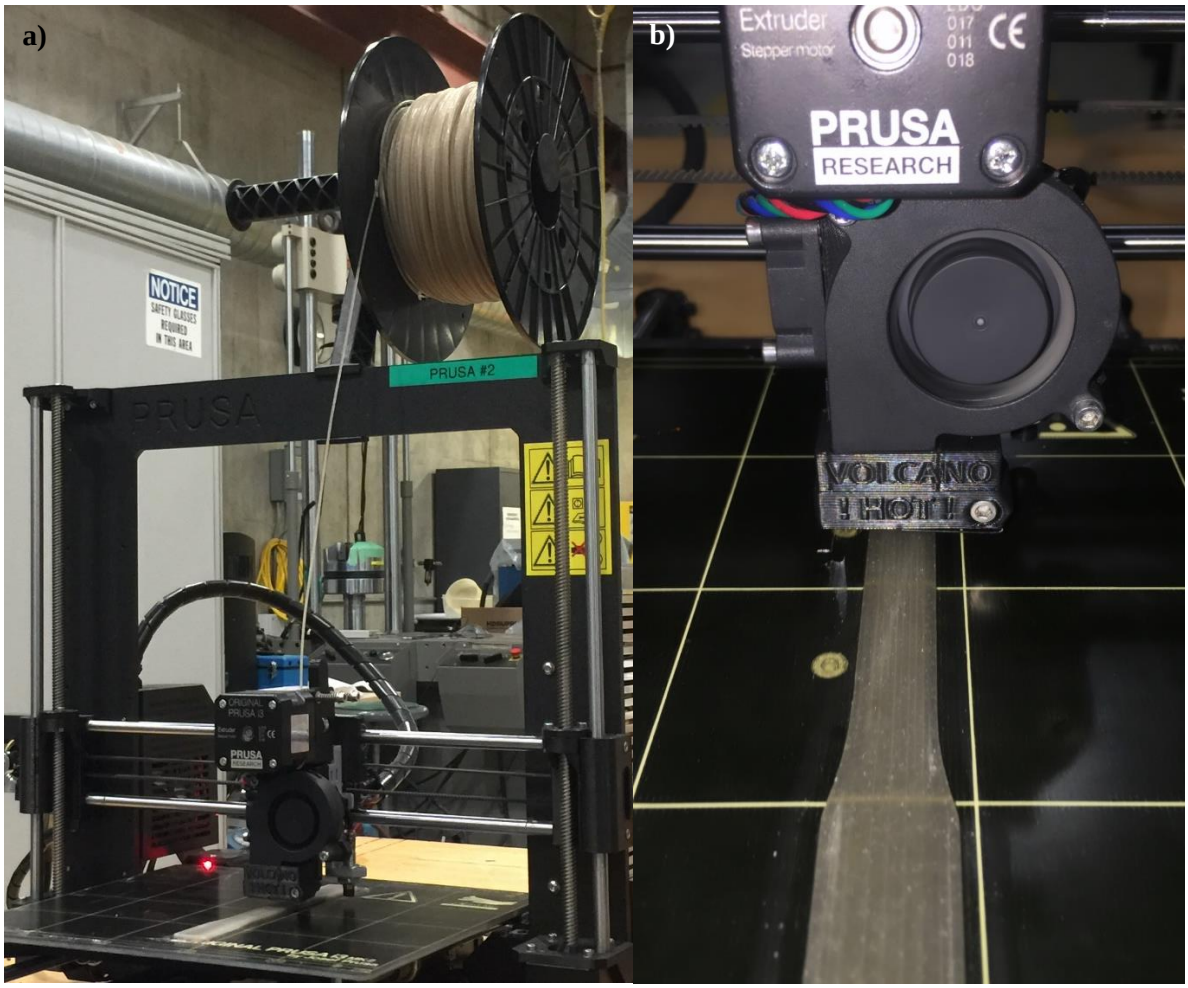

Figure 34. Coupon manufacturing: (a) Prusa Mk2 i3; and (b) closeup view of ASTM D638-14.

2.2.7 Micrographs of Composite Coupons and Filament

The images were produced using a standard compound microscope to image the fibers reinforced in the coupon beads. Two fibers can be seen to be parallel with a bead and each other.

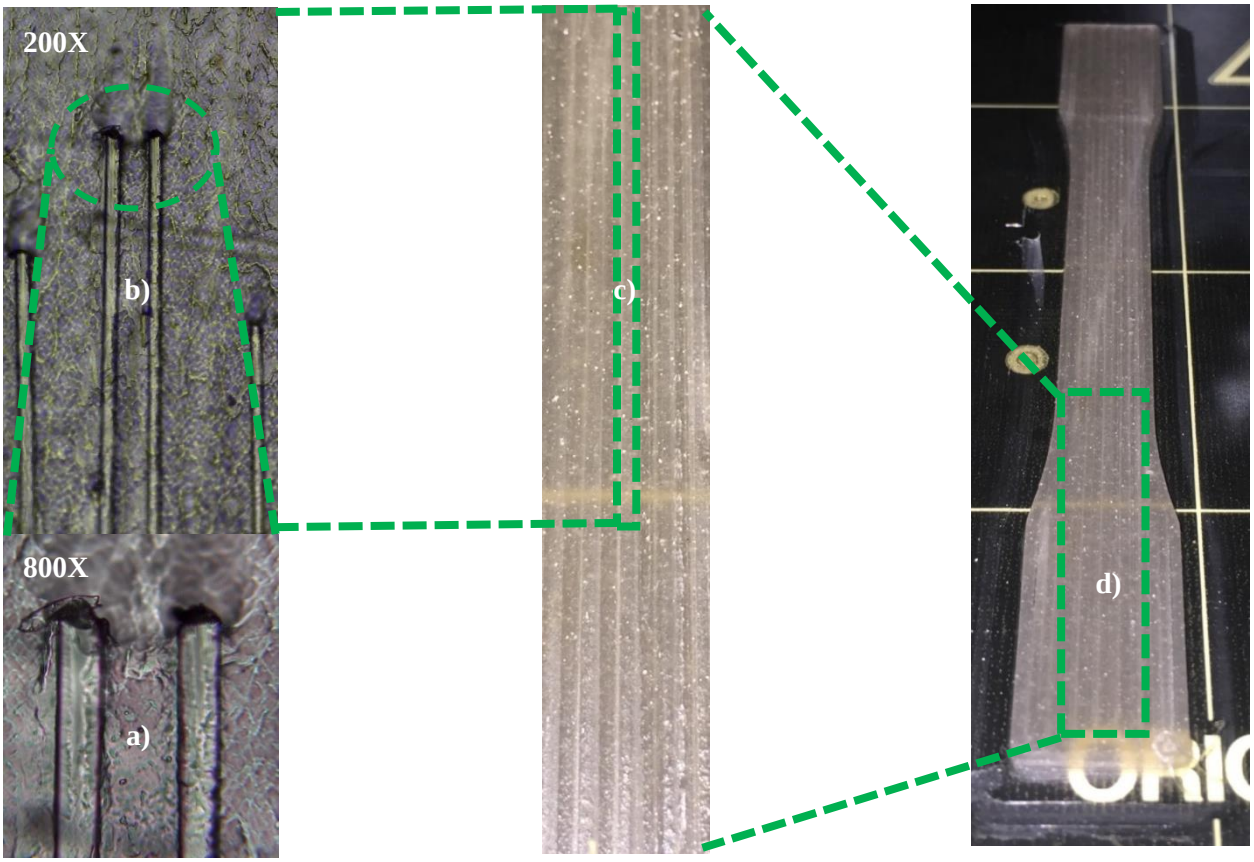

Figure 35. Micrographs: (a) 800X; (b) 200X; (c) 1X cropped; and (d) 1X uncropped.

Visible ‘drag’ marks can be seen in the PLA matrix above the fibers indicating the direction in which the bead was deposited during fabrication. Additionally, the ends of the fibers can be seen to be slightly irregular from the grinding process with some epoxy residue still present in small amounts. It has been observed that many of the fibers become alligned to be in the direction of the printed bead. This can be attributed to the narrowing of the nozzle and the inherent velocity profile, previously mentioned, due to shear effects within the barrel during the first extrusion to allign fibers in the filament. Furthermore, during the second extrusion the 1.75 mm filament is decreased down to 1.2 mm beads with additional no-slip conditions occurring at the nozzle walls: promoting fiber allignment with the flow directuion. This is extremely beneficial to the tensile strength as the fibers are alligning with the direction of the applied load.

The SEM and Mirco-CT images were provided by McGill University for the recycled composite filaments manufactured.

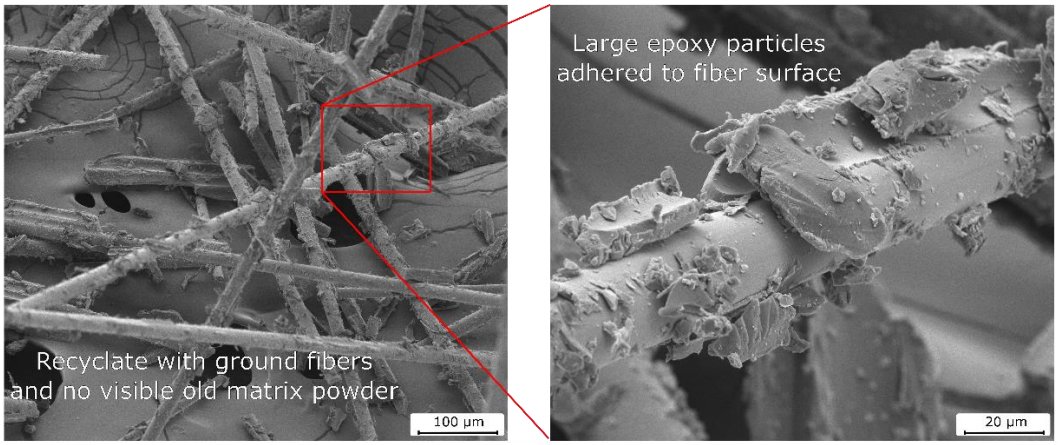

Figure 36. SEM Micrograph showing thermoset epoxy residue on recycled fiberglass.

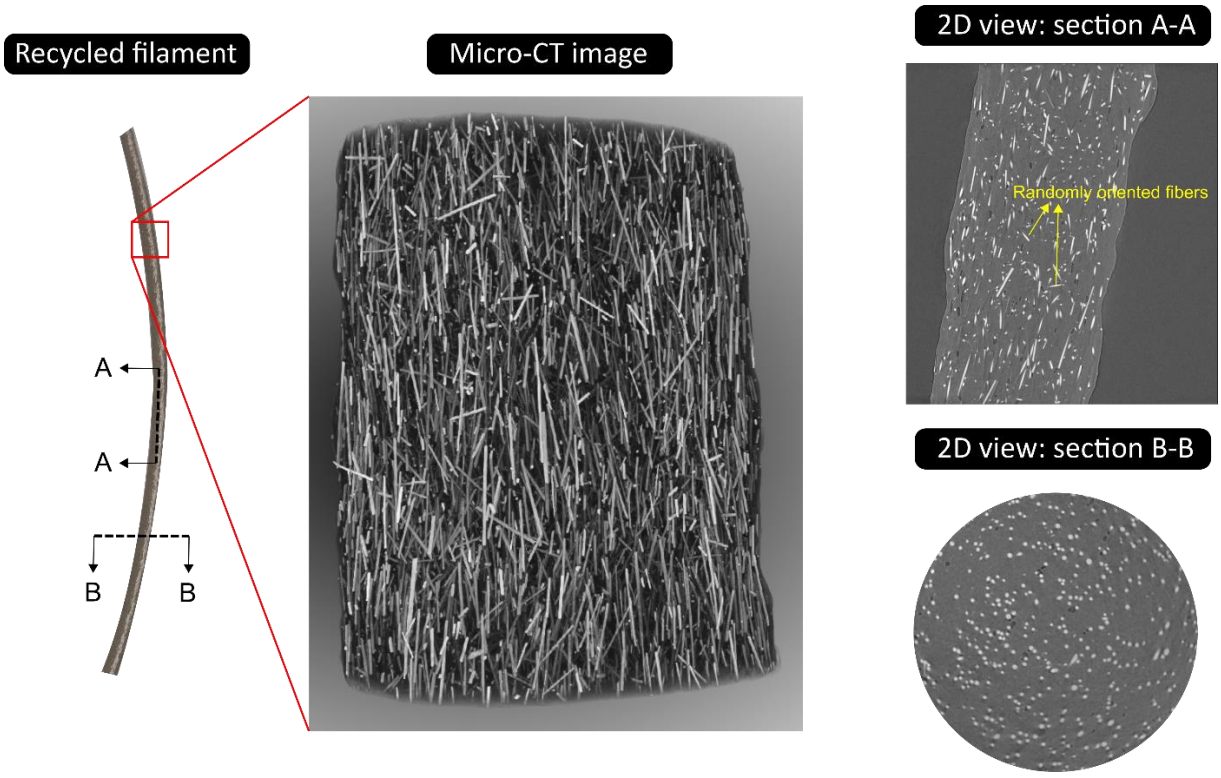

Figure 37. Micro-CT image of RFG-PLA filament.

The thermoset epoxy residue can be clearly seen on fibers of the recycled fiberglass composite. The long fibers can be seen in large amounts in each of the figures. Some of the glass fibers have been found to be up to 1 mm in length and can be seen with the unaided eye with a bright light source.

2.2.8 Final Coupons

This section presents Figures 38-42 showing the 40 total coupons manufactured for this study: 10 coupons for pure PLA, 3% RFG-PLA, 5% RFG-PLA, and 10% RFG-PLA. Each coupon takes approximately 30 minutes to print with a 1.2 mm nozzle and the previously summarized printing parameters. This yields a total print time of approximately 20 hours total for the ASTM D638-14 coupons manufactured.

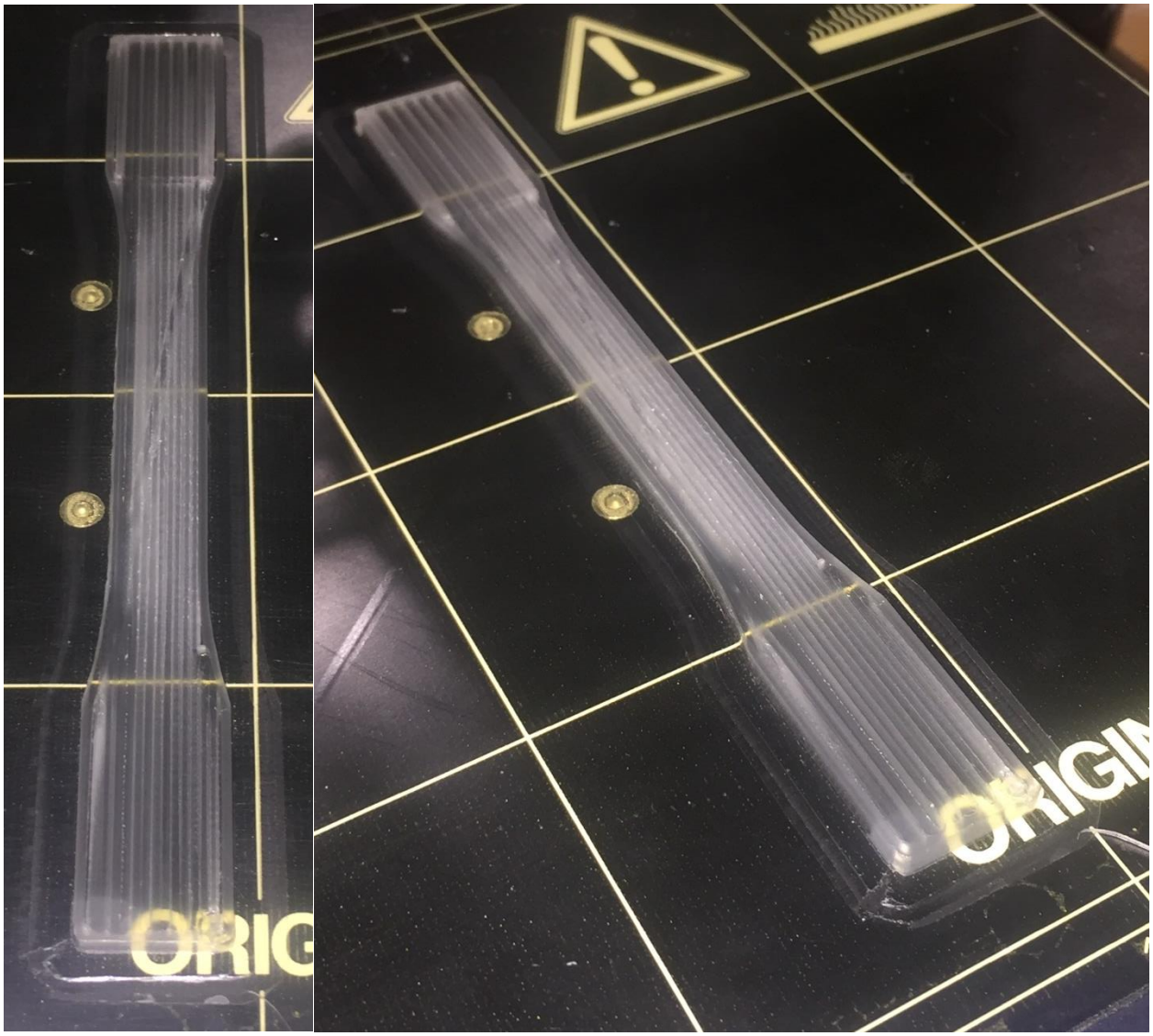

Figure 38. Pure PLA ASTM D638-14 coupon.

Figure 39. Final pure PLA coupons.

Figure 40. Final 3% critical fiber-length (3L-RFG-PLA) coupons.

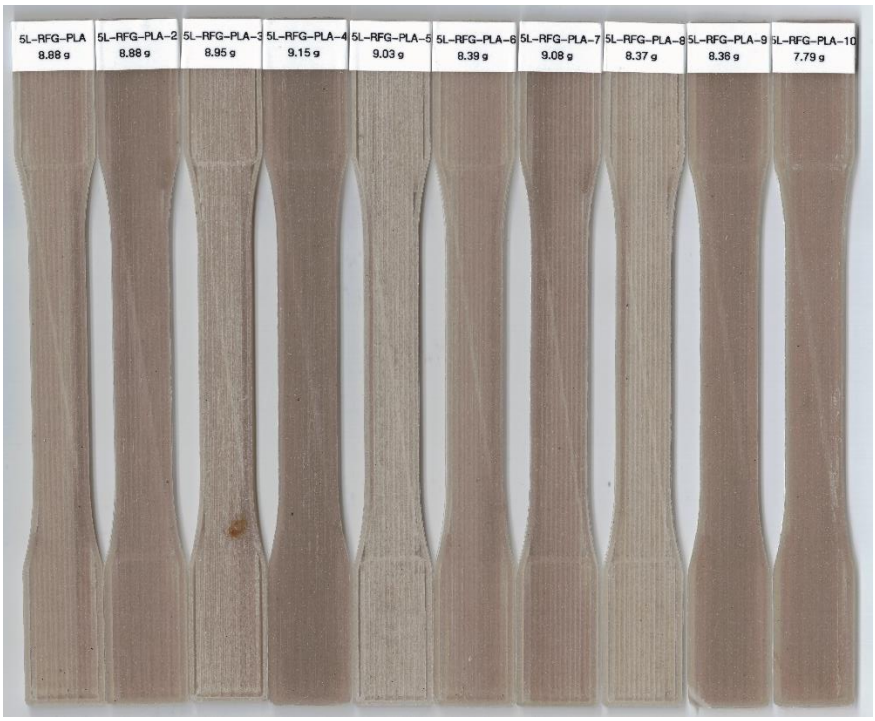

Figure 41. Final 5% critical fiber-length (5L-RFG-PLA) coupons.

Figure 42. Final 10% critical fiber-length (10L-RFG-PLA) coupons.

2.2.9 Results of Tensile Tests

All the below results have been provided by McGill University which summarize the results of the tensile tests for all the coupons previously shown.

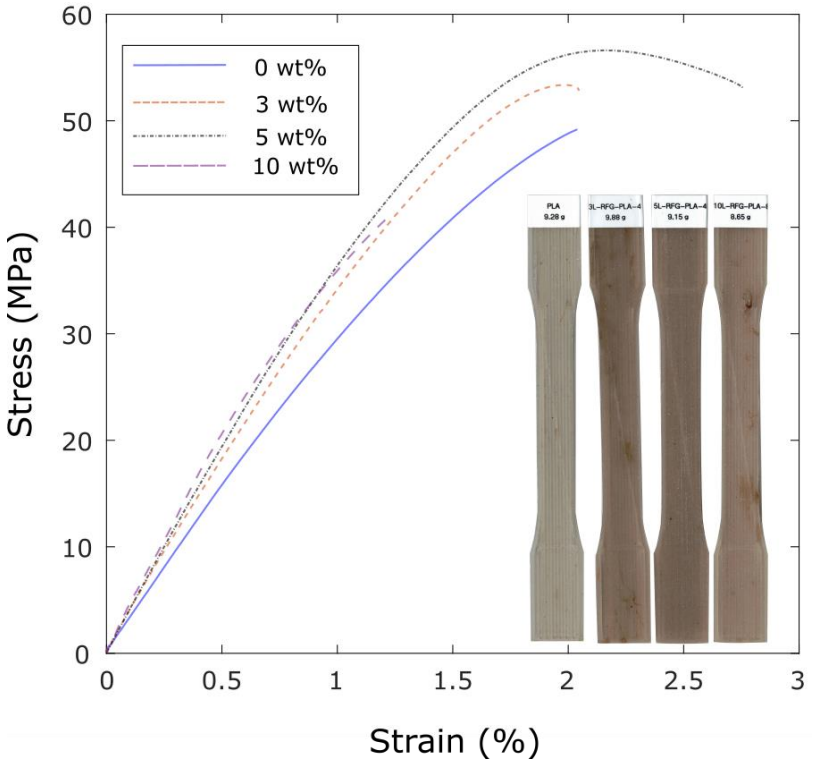

Figure 43. Stress-strain curves for the recycled fiberglass reinforced PLA coupons.

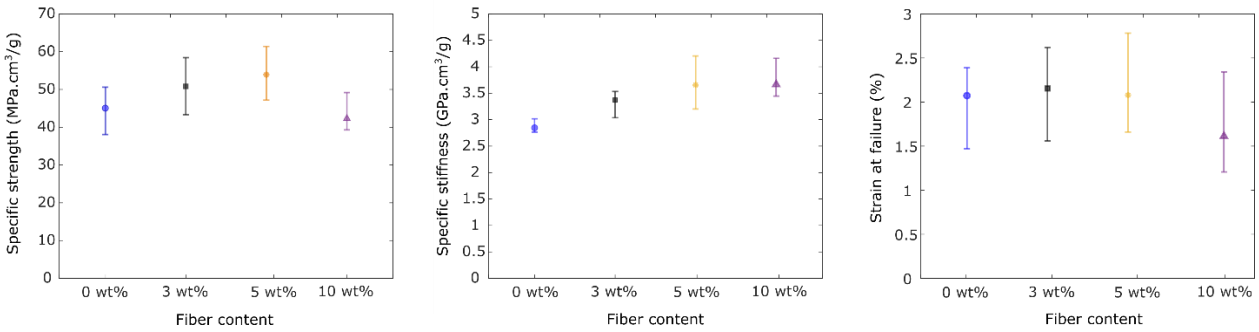

Figure 44. Tensile properties of the recycled fiberglass reinforced PLA coupons.

The table provides a summary of the mechanical properties of each material and the plots show the comparison of non-reinforced versus reinforced materials.

Table 3. Summary of the mechanical properties for each material.

Fiber content	Mean specific strength ($MPa.cm^3/g$)	Mean specific stiffness ($GPa.cm^3/g$)	Mean failure strain (%)	Strength SD	Stiffness SD	Failure strain SD
0 wt %	45	2.84	2	4	0.1	0.3
3 wt %	50.8	3.36	2	5.1	0.2	0.3
5 wt %	54	3.66	2	5.4	0.5	0.4
10 wt %	42.3	3.7	1.16	3.7	0.3	0.4

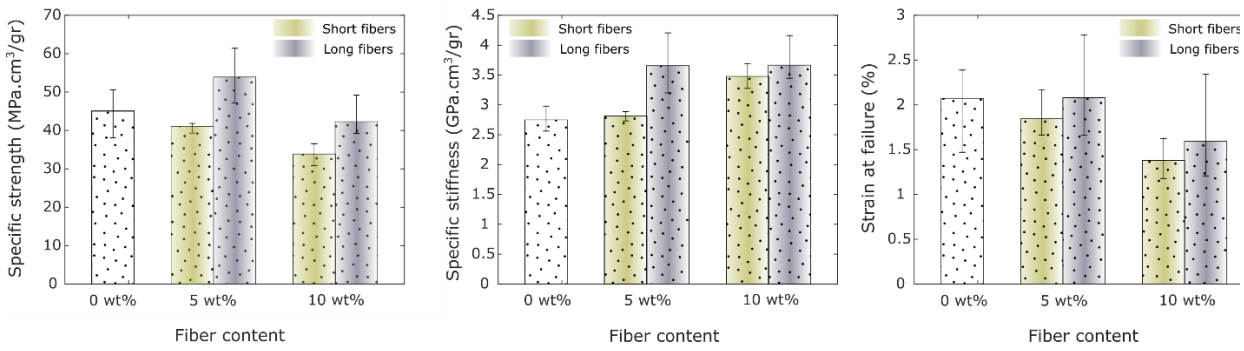

Figure 45. Comparison of the mechanical properties of pure PLA, short and long fibers.

In summary, it was found that the long fiber reinforced PLA provided a 20% increase in tensile strength and a 28% increase in the stiffness compared to the pure PLA specimens. It appears that the 5% wt RFG-PLA material performed the best in terms of the specific strength with an average value of 54 MPa. It was shown that both recycled short and long fiberglass from end-of-life wind turbine blades enhance the stiffness of 3D printed components. In addition, the long fibers allow for a clear improvement in the tensile strength when compared to pure PLA parts. This material could also be utilized in injection molding applications by using a single-screw extruder with a die with a desired geometry. Applications that require high stiffness could benefit from this material for various applications. Weight savings for specific applications in addition to high performance parts for rapid prototyping could be a suitable application of this material. Further ASTM standard testing can be performed to gather a more complete dataset on the mechanical performance of these materials.

2.3 Draping Analysis for Flexible 3D Printed Textiles

To address issues surrounding the large textile waste present in the fashion and apparel industry, potential uses for flexible thermoplastic textiles was investigated. To characterize the material properties, a method to study the draping behaviour was initiated. This brief section of the report outlines some of the preliminary progress with the draping apparatus and the simple proof of concepts. This is a project performed in collaboration with the fashion department within the Faculty of Communication and Design (FCAD). Assistant professor Dr. Danielle Martin from the fashion department is a collaborator on this project and will use results for a future project. In theory, these thermoplastic textiles could be manufactured and then recycled at the end of their life using the filament extrusion system developed in Section 2.2.

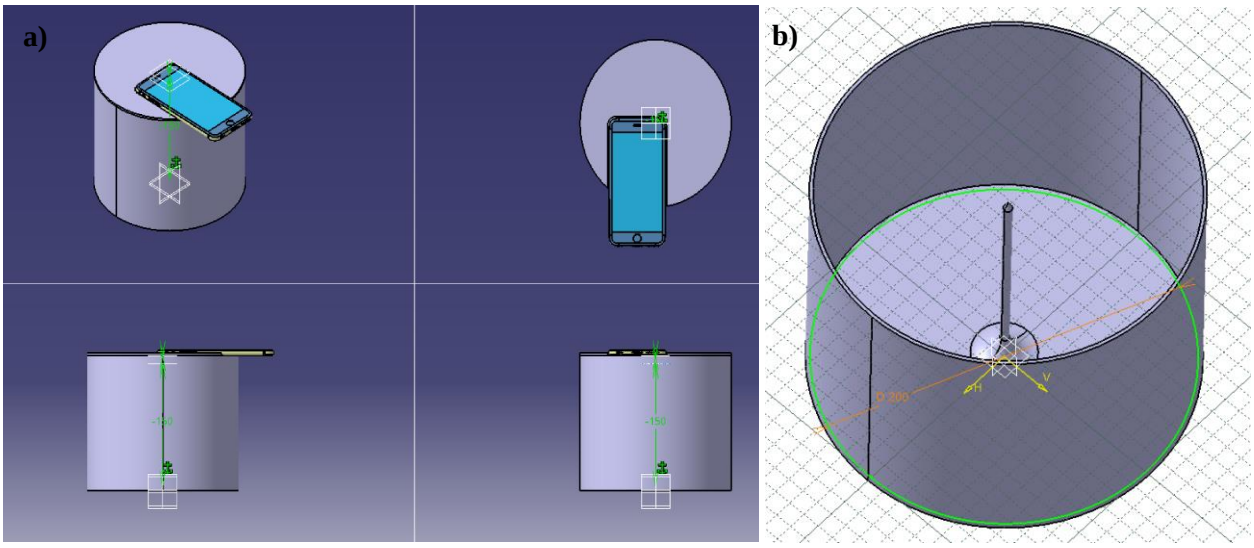

Figure 46. Draping apparatus: (a) multi-view; and (b) isometric view.

A simple prototype intended to easily photograph the draping behaviour of circular textile specimens or ‘coupons’ was designed to begin the draping investigation of 3D printed flexible textiles. This prototype is based off a *Cusick Drape* Tester [12]. The prototype was manufactured in the FRAMES lab on our ANYCUBIC CHIRON 3D printer out of PLA. It has a 200 mm base diameter and can therefore have a maximum specimen with the same dimension. For testing, a 150 mm and 100 mm diameter specimen geometry were used. Once the image is taken, it can be exported to either computed aided design (CAD) software such as CATIA V5 or to a MATLAB line detection script. This prototype simply acted as a proof of concept and the next iterations will use an integrated camera and lighting system. The use of a webcam, microcontroller and a custom-made code will be investigated for the next prototype.

The figures presented show initial 100 mm diameter test specimens to conduct draping analysis studies for textiles with various infill geometry and density. The three test infill patterns were selected using traditional composite nomenclature for quasi-isotropic and cross-ply.

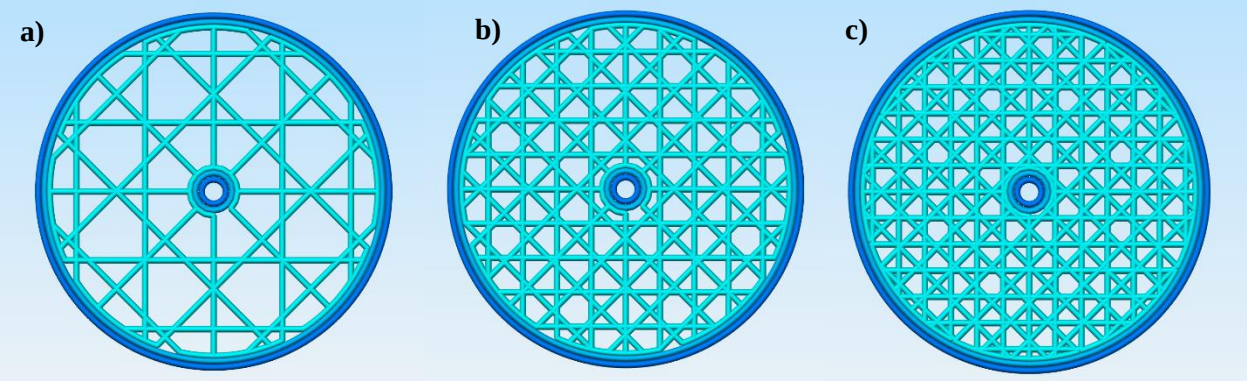

Figure 47. ‘Quasi-Isotropic’ pattern: (a) 25%; (b) 50%; and (c) 100% infill.

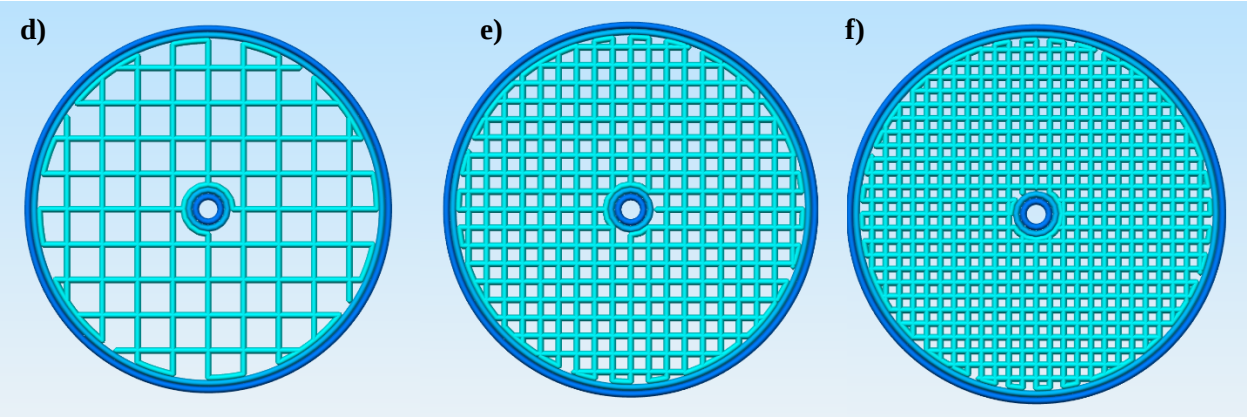

Figure 48. ‘Cross-Ply’ pattern: (d) 25%; (e) 50%; and (f) 100% infill.

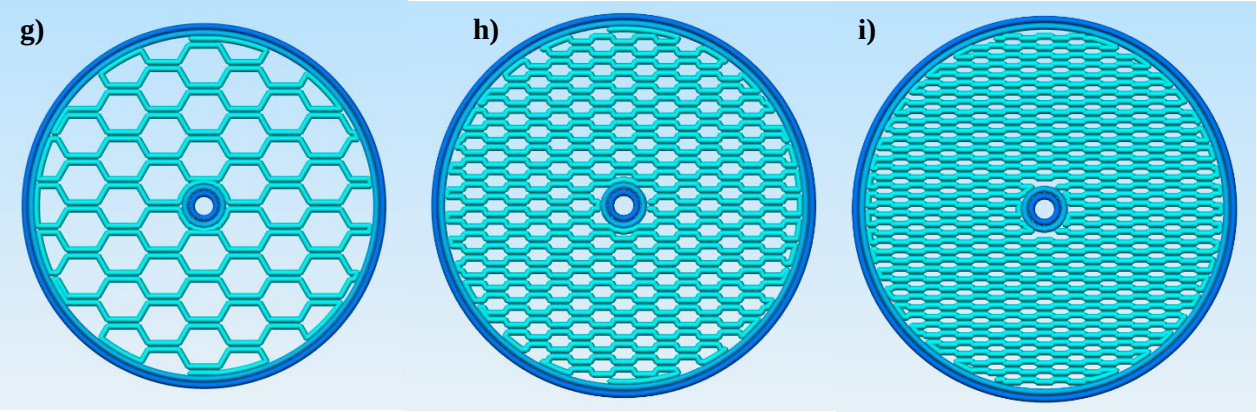

Figure 49. ‘Honeycomb’ pattern: (g) 25%; (h) 50%; and (i) 100% infill.

The varying degree of infill directly affects the draping characteristics of the textile specimen. Specimens were printed using a flexible material known as thermoplastic polyurethane (TPU). Images were taken using the draping prototype and imported into CATIA V5 as an immersive sketch. The outline of the draped geometry was extracted and created into a surface. The surface area of this region was measured and used to determine the draping coefficient (DC) of the textile. This measured area is area of the undraped textile.

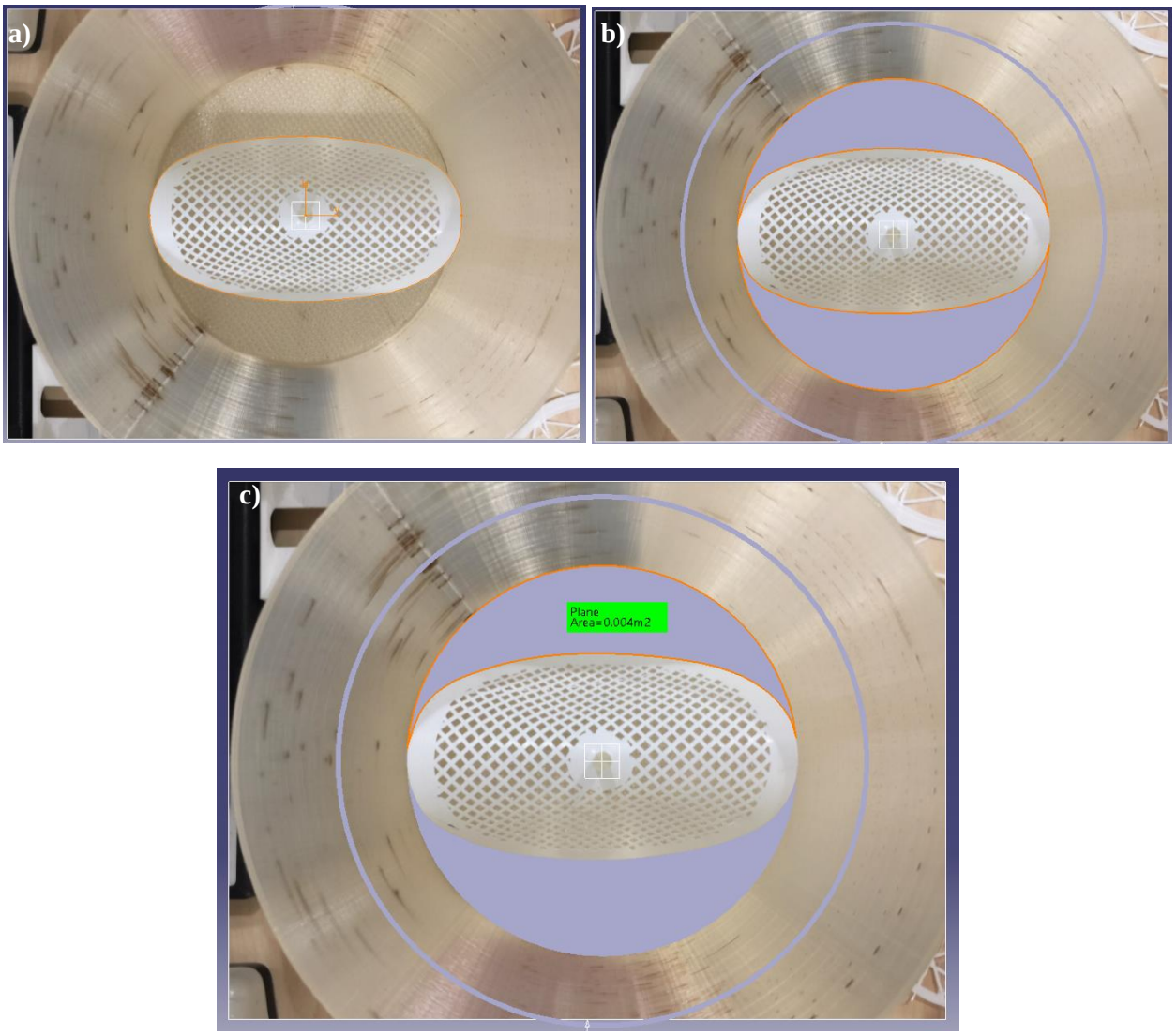

Figure 50. Test #1: (a) imported image; (b) generated undraped area; and (c) half of undraped area.

To determine the draping coefficient of the textile, the surface areas measured are input into Eq (4). The draped area is the area of the textile itself and the undraped area is the remaining area surrounding this draped region [13].

$$Draping\ Coefficient = \frac{Draped\ Area}{Undraped\ Area} \tag{4}$$

$$DC = \frac{0.017671458 - 0.008}{0.017671458} = 1 - \frac{Outer\ Ring\ Area}{Undraped\ Area} = 0.547 = \mathbf{54.7}\%$$

(for 50% infill [0,90] 'cross-ply' with 5 perimeters)

It was determined that the draping coefficient of this cross-ply specimen with 50% infill was 54.7%. This provides a metric to compare this textile with other geometries and infill densities. The infill is proportional to the draping coefficient; however, the exact nature of the proportionality requires rigorous testing. A second test was completed in this initial study to investigate the draping coefficient of another textile geometry with a lower infill percentage.

A quasi-isotropic textile with 25% infill was studied using the same method outlined in test #1. The resulting draping coefficient is shown below and can be seen to be lower than the previously tested specimen.

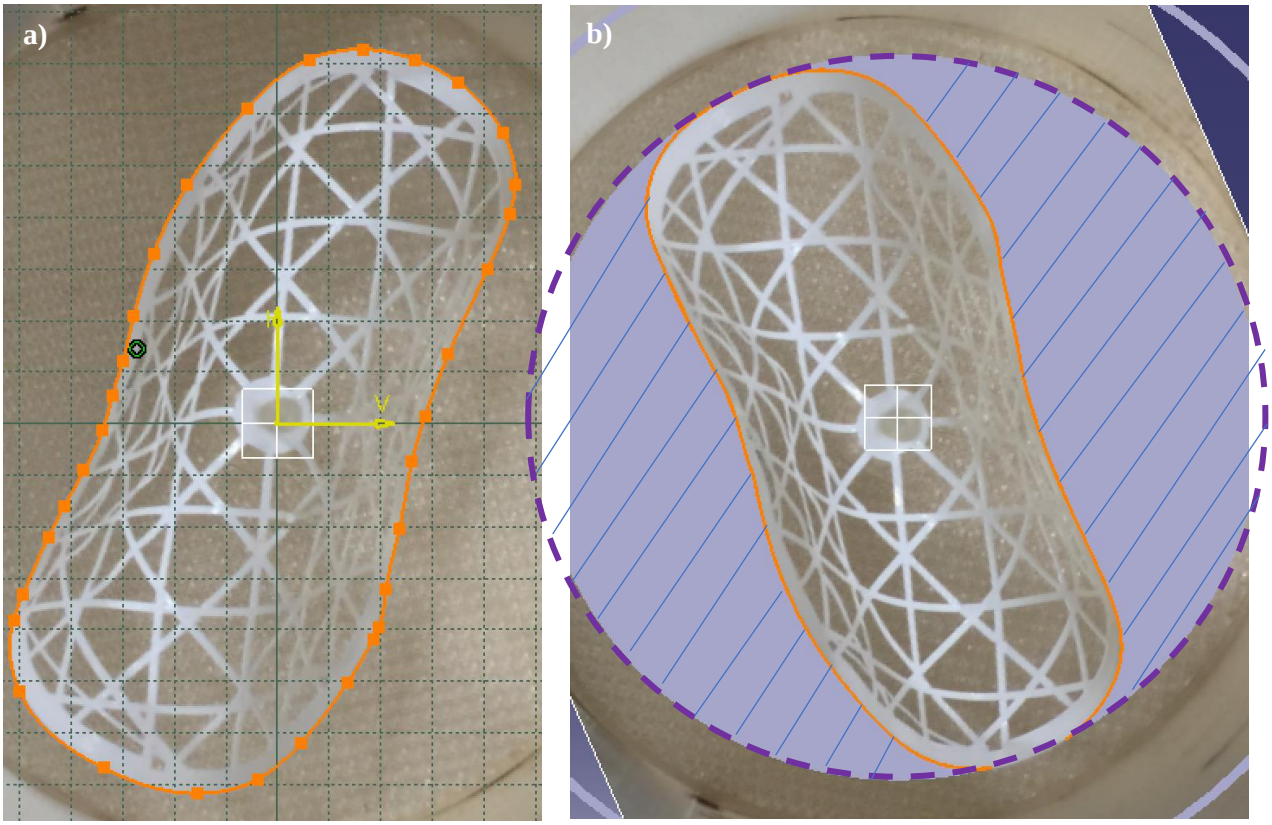

Figure 51. Test #2: (a) spline generation; and (b) undraped area generation.

$A_{OR} = 0.009\ m^2$ (area of the outer ring shown in light purple)

DC = 0.491 = 49.1% (for 25% infill [0,90,45,-45] 'quasi' with 5 perimeters)

Between these two samples, it can be clearly seen that their draping 'modes' vary with visible regions of deformation. The second specimen has a lower draping coefficient with 49.1% compared to 54.7%. There are visible sections that are concave relative to its draping path. The use of a MATLAB line detection script can identify the concave and convex regions and provide more data to explain the nature of the draping textiles. A high draping coefficient (DC) corresponds to a stiffer the textile and hence drapes to a lesser degree.

An additional draping test procedure was investigated using standard washers and nuts as weights to amplify the draping characteristics of the small textile coupons. Based on the placement of the weights, different draping ‘modes’ can be found with an associated number of ‘nodes’. The textiles can be observed to have symmetric or asymmetric static states. Both the cross-ply and honeycomb infills were observed to have two distinct modes. By keeping the positions of the weights constant across various textile geometries and infill density, a more complete draping characterization can be completed.

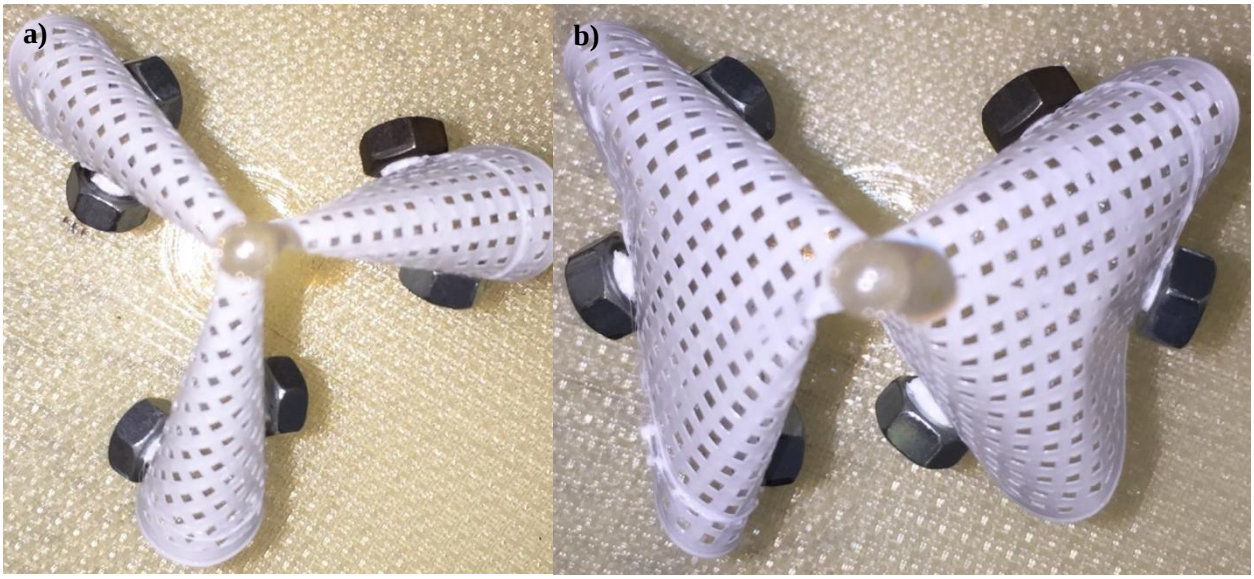

Figure 52. Test #3: (a) 3 nodes; and (b) 2 nodes with symmetry.

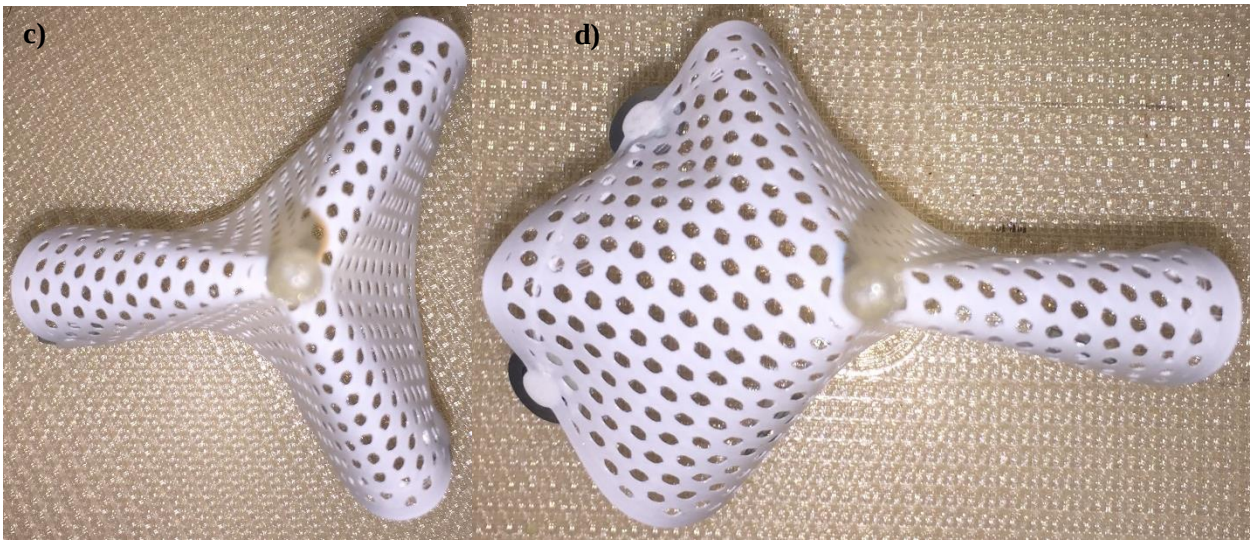

Figure 53. Test #4: (c) 3 nodes; and (d) 2 nodes with asymmetry.

3.0 Conclusion

In conclusion, the results of this report found that the use of recycled fiberglass recovered from end-of-life wind turbine blades enhances the mechanical performance of a thermoplastic matrix. It was found that the long fiber reinforced PLA provided a 20% increase in tensile strength and a 28% increase in the stiffness compared to the pure PLA specimens. The increased strength and stiffness can allow the material to be used in smaller quantities when replacing a given thermoplastic material. This material could be beneficial for both rapid prototyping and application specific products. In addition to the issues faced with the waste management of wind turbines, so too is the textile waste created by the improper disposal of clothing. Wind turbines provide an excellent source of renewable energy; however, neglecting the end-of-life portion of its lifecycle is extremely dangerous and wasteful. Every year, tens of thousands of tons of wind turbine waste is created from decommissioned blades. [1]. Industrial recycling solutions such as the one outlined in this report must be implemented on a large scale to prevent this waste from being incinerated and adding to CO_2 emissions. This report shows a potential use of this material to create an end-of-life bio-thermoplastic that can be used for various applications which could extend its lifecycle much further. A recycling plant for wind turbine blades could theoretically be powered by wind turbine blades to maintain a self-sustaining circular economy. Once these blades are decommissioned, they would join the other decommissioned blades. However, less invasive renewable energy sources are available so a complete lifecycle analysis must be conducted to determine the most optimal solution for the environment. In addition, to address the issues faced with improper disposal of clothing, a material characterization method for analyzing the draping behaviour of flexible 3D printed textiles was initiated. These 3D printed textiles could be processed, recycled and reused as new textiles. The study provided a proof of concept to systematically study the draping of a textile to characterize the material and compare it with existing fabrics. Pairing an extrusion system with 3D printing allows for the most rapid development of both a specialized material and product. Looking to the future of the textile industry, it is crucial that sustainable recycling and manufacturing processes are used to create a better future for the generations to come.

4.0 References

[1] P. Liu and C. Y. Barlow, "Wind turbine waste in 2050," *Waste Management ,* vol. 62, pp. 229-240, 2017.

[2] C. Álvarez-Chávez, S. Edwards, R. Moure-Eraso and K. Geiser, "Sustainability of bio-based plastics: general comparative analysis and recommendations for improvement," *Journal of Cleaner Production,* pp. 47-56, 2011.

[3] The Sustainable Biomaterials Collaborative, "Guidelines for Sustainable Bioplastics," 2009.

[4] A. Morão and F. de Bie, "Life Cycle Impact Assessment of Polylactic Acid (PLA) Produced," *Journal of Polymers and the Environment,* 2019.

[5] NatureWorks, "Ingeo™ Biopolymer 4043D Technical Data Sheet," Minnetonka.

[6] M. P. Groover, "Shaping Processes for Plastics: Extrusion," in *Fundamentals of Modern Manufacturing* , John Wiley & Sons INC., 2010, pp. 268-273.

[7] A. Rahimizadeh, J. Kalman, K. Fayazbakhsh and L. Lessard, "Recycling of fiberglass wind turbine blades into reinforced filaments for use in Additive Manufacturing," *Composites Part B,* vol. 175, 2019.

[8] FilaFab, "D3Dinnovations - PRO 350 EX," 2020. [Online]. Available: http://d3dinnovations.com/filafab/product/filafab-ex-350/. [Accessed 10 April 2020].

[9] Noztek, "Noztek Pro HT," 2020. [Online]. Available: https://www.noztek.com/product/noztek-pro-high-temperature-extruder/. [Accessed 10 April 2020].

[10] Keyence, "LS9030M Laser Micrometer," [Online]. Available: https://www.keyence.ca/products/measure/micrometer/ls-9000/models/ls-9030/. [Accessed 11 April 2020].

[11] A. Rahimizadeh, J. Kalman, R. Henri, K. Fayazbakhsh and L. Lessard, "Recycled Glass Fiber Composites from Wind Turbine Waste for 3D Printing Feedstock: Effects of Fiber Content and Interface on Mechanical Performance," *Materials (MDPI),* vol. 12, no. 23, 2019.

[12] E3D , "Volcano Hotend," [Online]. Available: https://e3d-online.com/volcano-upgrade-kit. [Accessed 10 April 2020].

[13] M. Kiron, "Cusick Drape Tester," Textile Learner, [Online]. Available: https://textilelearner.blogspot.com/2012/02/what-is-drape-cusick-drape-test.html. [Accessed 10 April 2020].

5.0 Appendix

Engineering Drawings

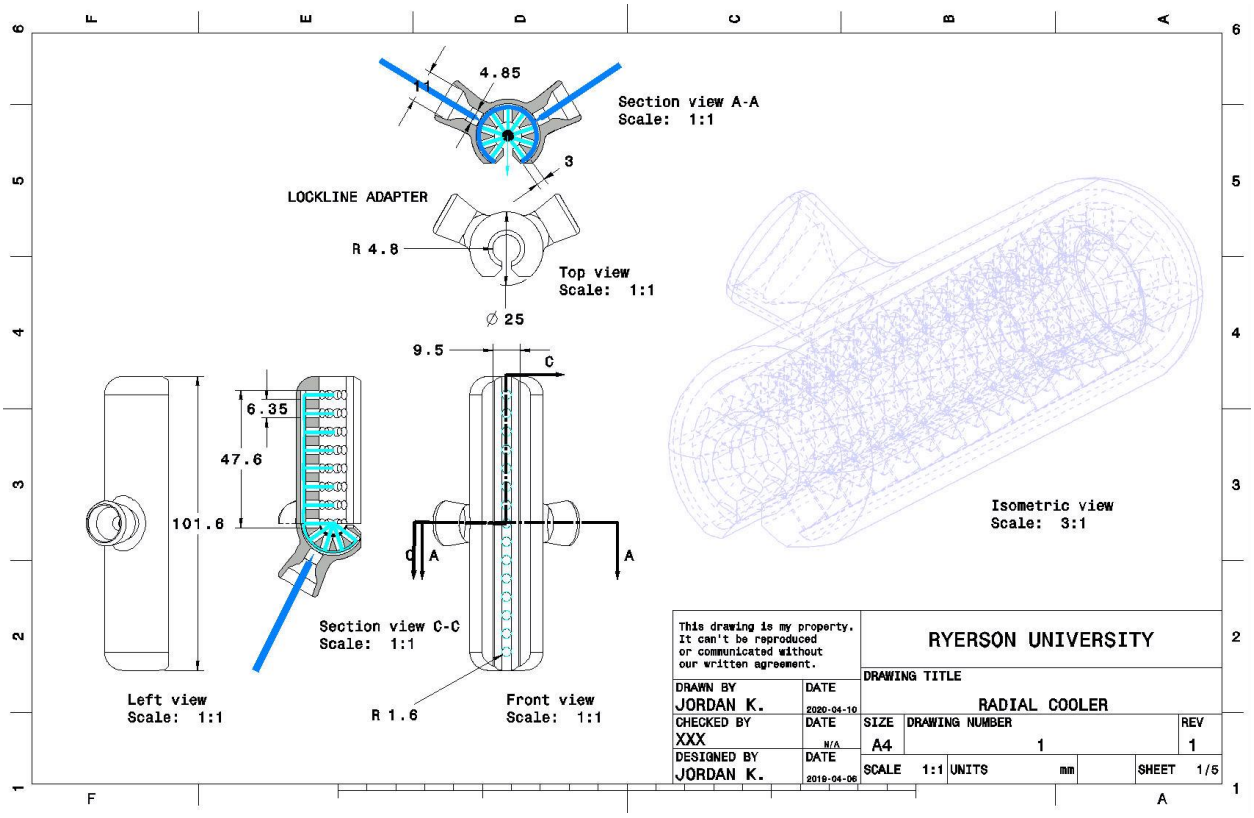

Figure 52. Radial air cooler.

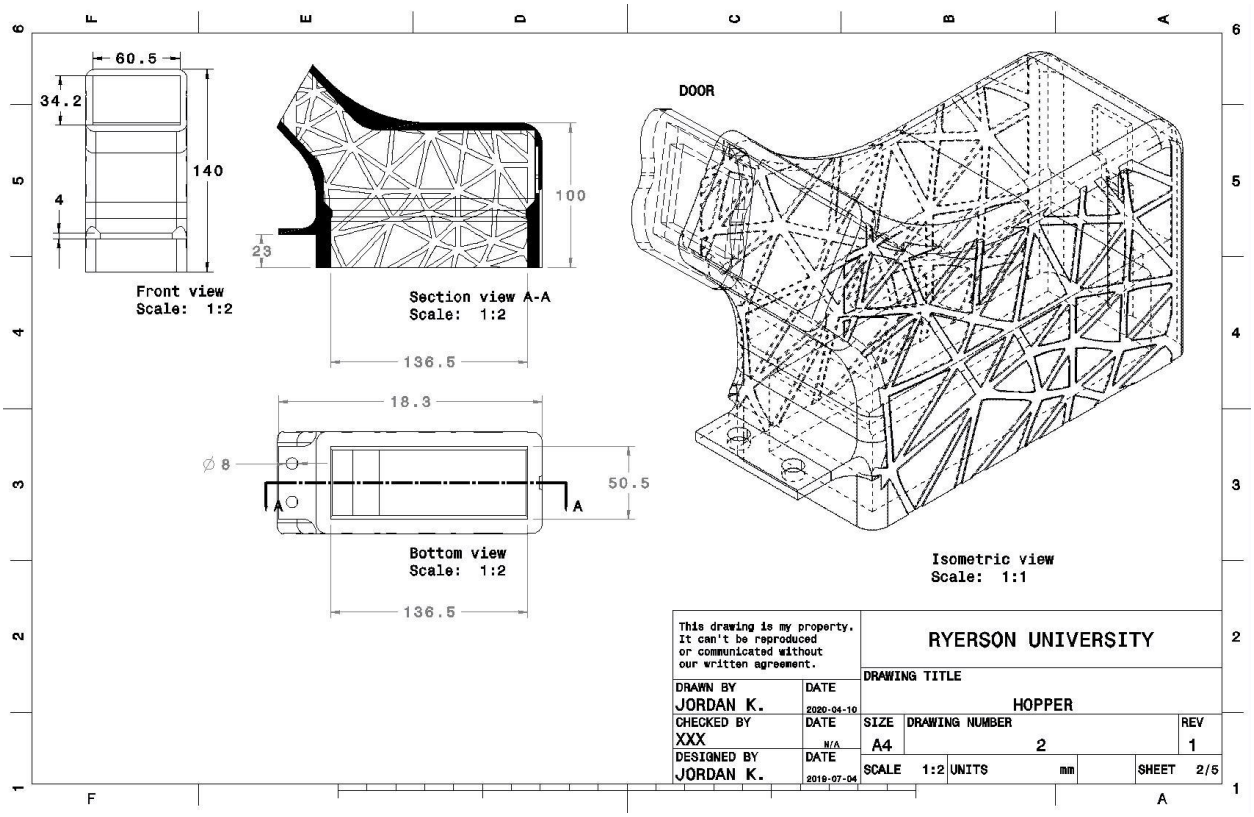

Figure 53. Hopper.

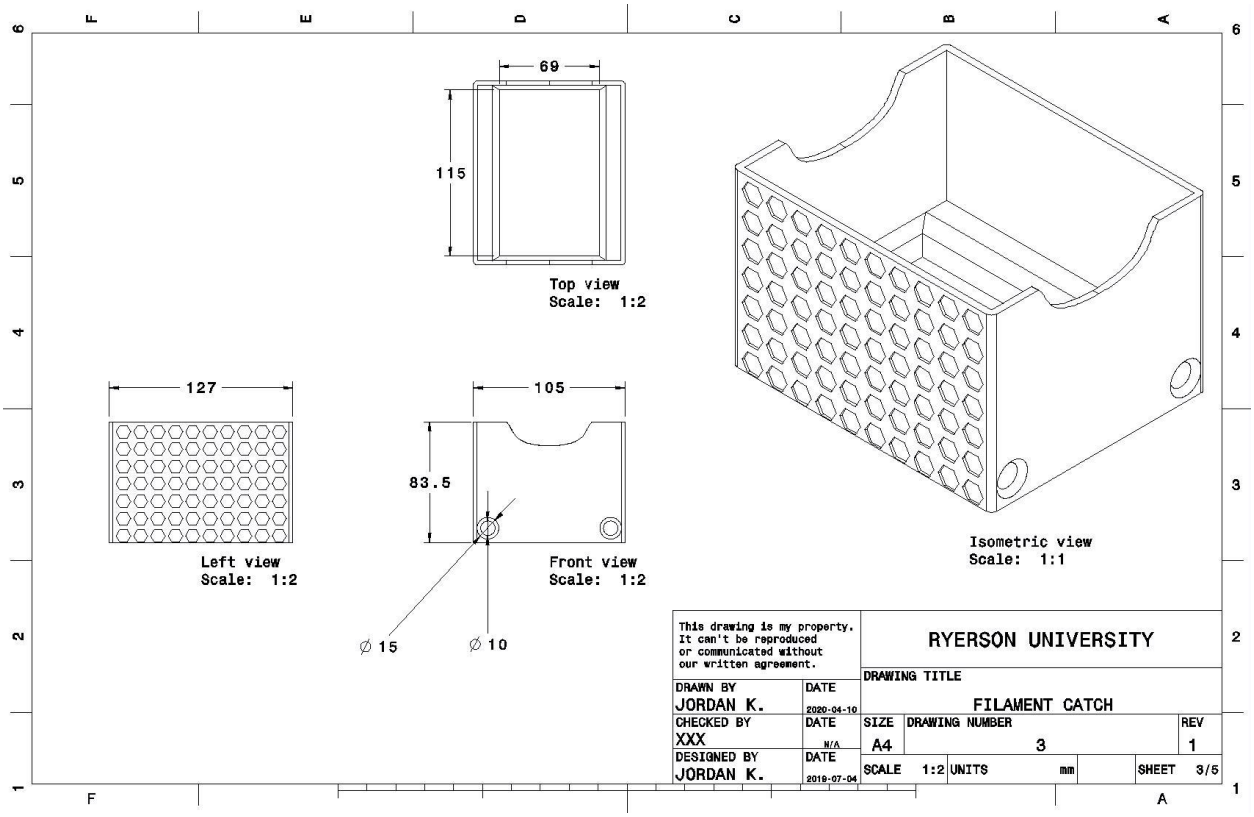

Figure 54. Filament catch.

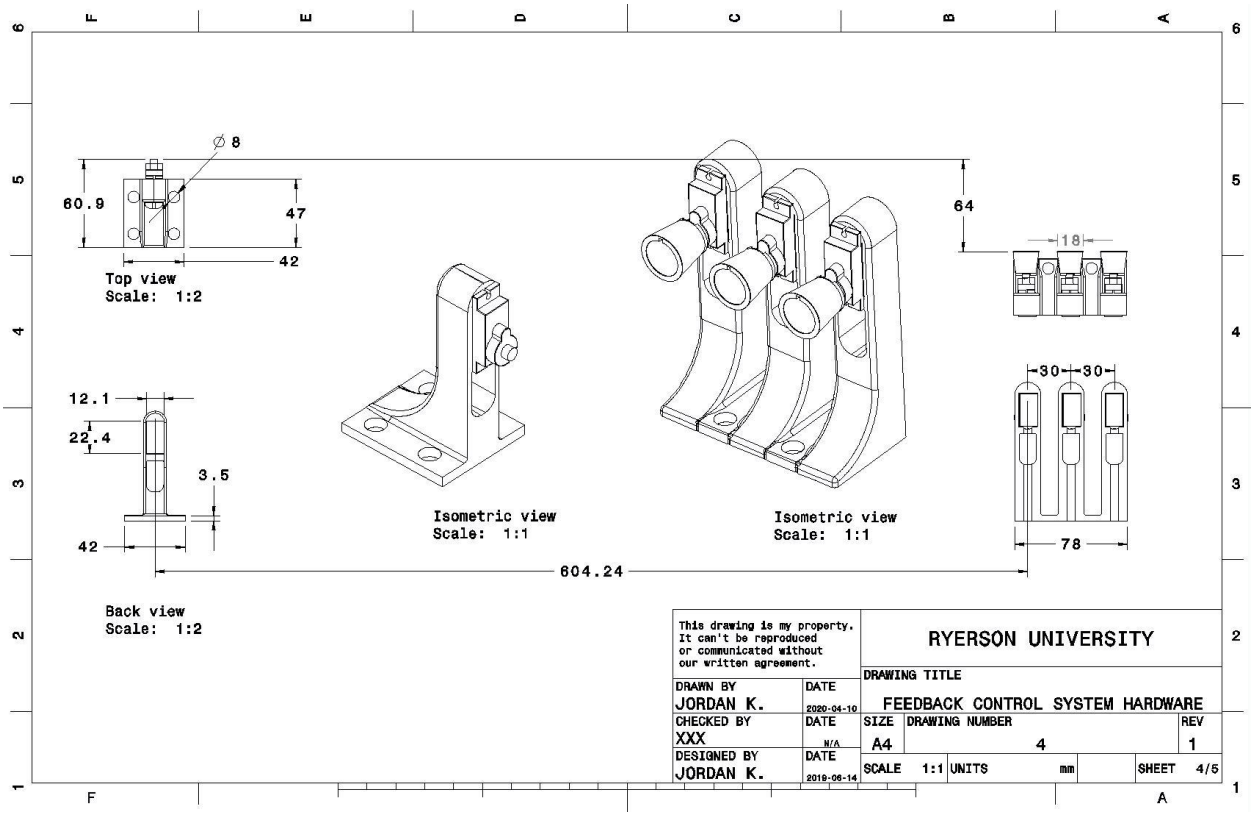

Figure 55. Feedback control hardware.

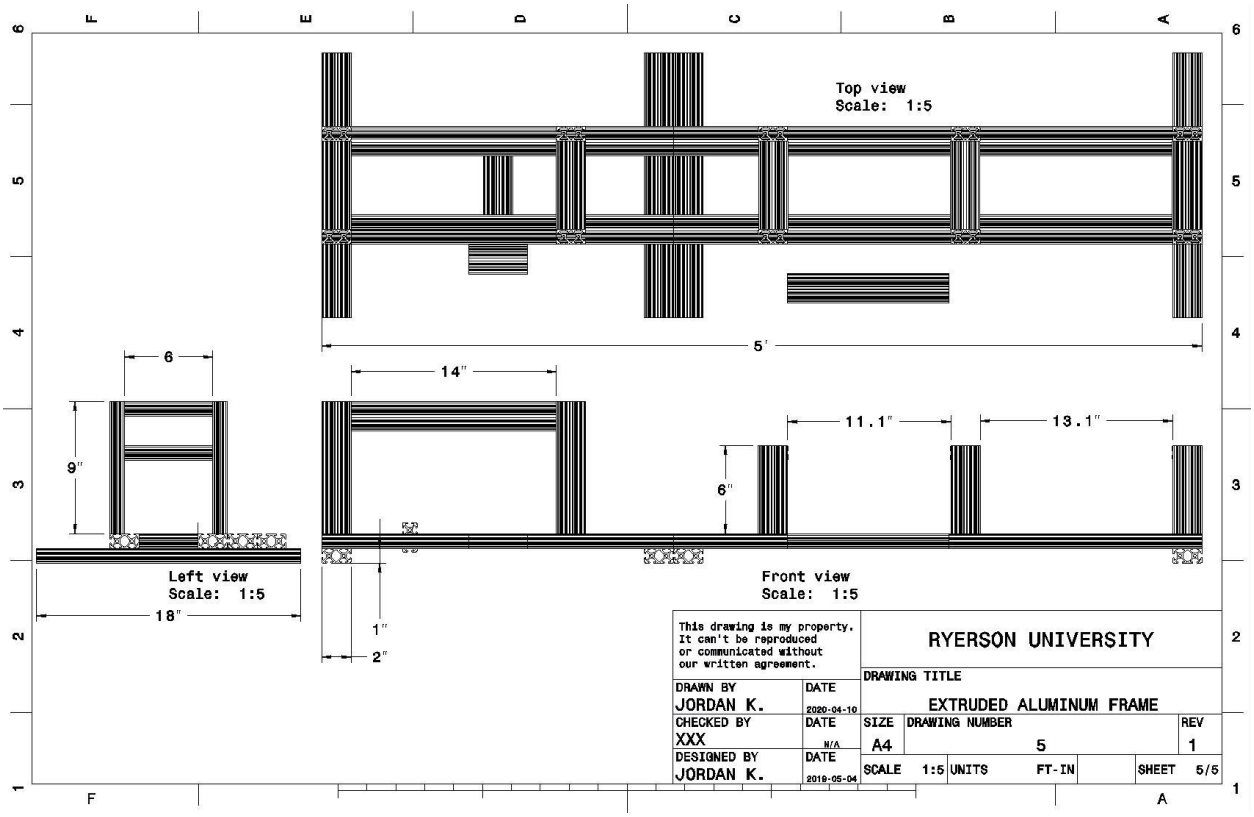

Figure 56. Extruded aluminum frame.